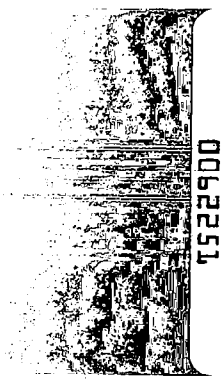

NASA Contractor Report 3495

Low-Authority Control Synthesis for Large Space Structures

J. N. Aubrun and G. Margulies

CONTRACT NAS1-14887
SEPTEMBER 1982

NASA

NASA Contractor Report 3495

Low-Authority Control Synthesis for Large Space Structures

J. N. Aubrun and G. Margulies
Lockheed Missiles and Space Company, Inc.
Palo Alto, California

Prepared for
Langley Research Center
under Contract NAS1-14887

National Aeronautics
and Space Administration

**Scientific and Technical
Information Branch**

1982

TABLE OF CONTENTS

ILLUSTRATIONS

TABLES

SUMMARY

This report deals with the problem of controlling the vibrations of large space structures by the use of distributed sensors and actuators. It specifically addresses the synthesis and implementation of Low-Authority Control (LAC) systems which arise when the above structural vibration controllers introduce only a moderate amount of damping (10 to 25 percent) in the structure.

The LAC gain synthesis is achieved by an exact algebraic optimization of a weighted quadratic cost function based on the fundamental LAC root-shift prediction formula. The cost function is the sum of two disparate design objectives, making its optimization a special case of a pareto-optimal design [1]. To broaden the applicability of the LAC synthesis procedure, the LAC theory has been generalized to arbitrary linear time-invariant systems which include general filter equations. The ensuing LAC synthesis procedure is then applicable to structures which already have some natural damping or some embedded attitude or structural control systems. In turn, this makes it possible to formulate and implement a sequential LAC synthesis procedure in which the perturbation method is applied sequentially in a manner analogous to the Newton-Raphson method. In this sequential procedure, the small amount of control synthesized at each step is embedded in the total dynamics, and the total system complex eigenvectors are recomputed for the next step.

The robustness of LAC active damping systems is examined and analyzed for realistic (finite-bandwidth) actuation systems. The stability characteristics of idealized and increasingly more realistic "structure-with-actuators" models is analyzed, leading to the fundamental LAC Stability Theorem for already damped structures equipped with both (finite-bandwidth) active and parallel-mounted passive actuators.

The LAC synthesis procedure is applied to the design of LAC controllers for vibration control of simply-supported rectangular plates for which frequencies and mode shapes are given analytically. Two aspect ratios are considered: (1) a 3:1 ratio plate, for which it is shown that at least 10 percent damping can be achieved in the first five modes with only three colocated sensor/actuator pairs, and (2) a $\sqrt{5/3}$:1 ratio plate, for which a similar objective is met with five sensor/actuator pairs. The special difficulty encountered for the second plate is the double-root frequencies of the fourth and fifth modes, leading to eigenvector indeterminacy. It is shown how the LAC sequential synthesis resolves that difficulty.

A newly conceived linear actuation device, the pivoted proof-mass (PPM) damper, is described and analyzed. It consists of a flexure-pivoted mass (proof-mass) driven electrodynamically in an ac-coupled fashion, dissipating structural energy through electrical network heat losses. Detailed scaling laws are presented for feasibility of extrapolation to large space structures.

INTRODUCTION AND OVERVIEW

In an earlier companion study [2], a general theory was developed for a class of control systems called Low-Authority Control (LAC) systems. When applied to structures, these are structural vibration control systems consisting of distributed sensors and actuators with limited damping authority, i.e., the control system is allowed to modify only moderately the natural modes and frequencies of the structure. This basic assumption, combined with Jacobi's root perturbation formula, leads to a fundamental LAC formula for predicting algebraically the root shifts produced by introducing an LAC control system. Specifically, for an undamped, open-loop structure, the predicted root shift $d\lambda_n$ is given by the quadratic form

$$d\lambda_n \cong -\frac{1}{2} \sum_{a,r} D_{ar} \quad \phi_{an} \quad \phi_{rn} \tag{i}$$

where the coefficient matrix D_{ar} is a matrix of (damping) gains, and ϕ_{an}, ϕ_{rn} denote, respectively, the values of the n^{th} mode shape at actuator station a and sensor station r.

Formula (i) may also be looked upon as (a set of) equations for the unknown gains D_{ar} if the $d\lambda_n$ are considered to be known (desired) root shifts or, equivalently, desired modal dampings. While an exact "inversion" of (i) does not generally exist, least-squares type solutions can be devised to determine the actuator control gains D_{ar} necessary to produce the required modal damping ratios. This determination of the gains is the synthesis of LAC systems, and is the basic problem addressed in the present study. In order to make such an LAC synthesis as useful as possible for practical application to large space structures, the LAC "scenario" has been generalized to arbitrary linear time-invariant systems of the form given in Eq. (1), p. 13, which, in this application, corresponds to already damped (controlled) structures equipped with distributed actuator/sensor systems, and for which the basic plant also

includes filter equations which may be used to model either sensor dynamics, actuator dynamics, state estimators, or any combination of them. In this most general case, the analog of formula (i) is the bilinear form

$$d\lambda_n \cong -\frac{1}{2} \sum_{a,r} D_{arn} \phi^A_{an} \phi^R_{rn} \qquad \text{(ii)}$$

where the terms $D_{arn} = D_{ar}(n)$ now depend on the mode number n and are generally complex, and where ϕ^A_{an}, ϕ^R_{rn} are, respectively, the a^{th} and r^{th} components of generalized actuator and sensor mode shapes ϕ^A_n and ϕ^R_n.

When the eigenvalues of the filter become large compared to those of the structure, it can be shown that the terms D_{arn} become independent of n, and (ii) then reduces to

$$d\lambda_n \cong -\frac{1}{2} \sum_{a,r} D_{ar} \phi^A_{an} \phi^R_{rn} \qquad \text{(iii)}$$

which is the most useful formula to use when sensor, actuator, or filter dynamics can be ignored or are already embedded in the system. Formula (iii) applies to already damped structures and is the basis for the general LAC synthesis procedure (LACSYS) and its iterative version (sequential LACSYS) discussed in the first chapter of this study.

The synthesis procedure is based on optimization of a weighted quadratic cost function related to (iii), and, in its implementation, is qualitatively similar to the classical optimal control gain synthesis procedures where a "dialogue" between the user and the free parameters of the system (in this case the weights in the cost function and the desired target modal damping ratios) is necessary to ensure that the control objectives are met. Even though synthesis of the control gains (for each set of specified weights and desired dampings) is achieved by exact linear algebraic processes, the resultant root shifts will only approximate the

desired ones because of the approximations inherent to the perturbation method employed. To improve the accuracy of the process, the perturbation method is applied sequentially in a manner analogous to the Newton-Raphson method. At each step, the small amount of damping due to the synthesized gains is "embedded" in the total dynamics, and the total system (complex) eigenvectors are recomputed. Because the synthesis procedure is applicable to already damped systems, it can indeed proceed in small steps such that the eigenvector shifts corresponding to the incremental damping added at each step remain small. This is particularly useful for the case of multiple roots for which the corresponding eigenvector indeterminacy produces large eigenvector shifts when damping is introduced.

The second chapter deals systematically with the robustness of LAC active dampers. Robustness is that quality of a controller of remaining stable in the presence of parameter variations in the structure and/or control system parameters. For example, a stability condition independent of mode shapes and frequencies, such as the negativity of all root shifts in the fundamental LAC formula (i) for the case of colocation (a = r), is an example of robustness when idealized (i.e., infinite bandwidth) actuators and sensors are used. The generalized LAC theory developed in the first chapter makes it possible then to examine various stability characteristics of idealized and increasingly more realistic (finite-bandwidth) systems, starting from ideal dampers in undamped and damped structures, actual active or actual passive dampers in undamped and damped structures, to the final case of both actual active and passive dampers in damped structures. The different cases considered lead to the final Stability Theorem for LAC active dampers in the presence of both natural structural damping and parallel-mounted, device-implemented passive damping.

The third chapter is devoted entirely to an application of the LAC theory in order to illustrate the LAC synthesis procedure. To this end, the structural model used is that of a simply-supported rectangular plate. For this model, the availability of analytic expressions for its frequencies and mode shapes

alleviates the need for finite-element models and their attendant numerical data-processing pitfalls. The 3:1 aspect ratio plate is treated first, and it is shown how three actuator/sensor pairs can easily produce (at least 10 percent damping in each of the first five modes. The $\sqrt{5/3}$: 1 aspect ratio plate is treated next its characteristic feature being that its fourth and fifth modes correspond to a double-root. The sequential LAC synthesis procedure is applied again in this case and a complete tabulation is given for the desired dampings, modal weights, and cumulative LAC gains occurring at each step. For this plate, 5 actuator/sensor pairs are used to produce (at least) 10 percent damping in each of the first five modes.

The fourth and final chapter deals with the mechanization of LAC systems, and focuses in particular on the proof-mass actuator as the device closest to the linear analog of the gyrodamper studied previously in [1]. Proof-mass actuators operate by the principle of inertial reaction: they apply a force to a small mass (proof-mass) and the d'Alembert reaction force is transmitted back to the structure. While this concept is quite straightforward, its practical implementation leads to numerous mechanical difficulties (e.g., friction, suspension stiffness, nonlinearities, etc.).

Rather than attempting to model these various pathologies (which most often are not even reproducible in a systematic way), the approach was taken to place a control system around the actuator itself in order to force it to behave in the desired linear manner. Furthermore, a much cleaner mechanical design was obtained by approximating linear motions via a small-angle pivoting device, the pivoted proof-mass (PPM) actuator. An electrodynamically driven prototype was built and is described in this chapter, and detailed scaling laws are presented for feasibility of extrapolation to large space structures.

LIST OF SYMBOLS

a	actuator index
a	rectangular plate length
A	filter dynamic matrix
b	rectangular plate width
b	PPM actuator composite center of mass coordinate
b_o	unloaded PPM actuator center of mass coordinate
B	filter input matrix
c	active control gain of a generic damping actuator
c_a	active control gain of damping actuator a
c'	active contribution to damping
C	control gains matrix
d	PPM actuator attachment point coordinate
d	vector of selected damping gains for LAC synthesis
d_i	i^{th} component of d
$d\lambda_n$	root shift of the n^{th} root under LAC control
D	damping gains matrix or scalar gain
D_n	equivalent damping gain matrix with filtering
D_{ar}	element a,r of D
D_{arn}	element a,r of D_n
E	Young's modulus
f	actuator reaction force on structure
f_m	maximum PPM actuator output force
f_{opt}	optimal PPM actuator output force
f_e	PPM actuator electrodynamic force
f_{em}	PPM actuator maximum electrodynamic force

F	dynamic matrix
G	input matrix
h	rectangular plate thickness
H	measurement matrix
i	free index
i	imaginary symbol $\sqrt{-1}$
I	loaded PPM actuator centroidal inertia
I_o	unloaded PPM actuator inertia w.r.t. pivot
I_s	sectional inertia of uniform beam
j	free index
J	LAC cost function
K_b	PPM center of mass scaling parameter
K_f	PPM output force scaling parameter
K_I	PPM inertia scaling parameter
K_m	PPM mass scaling parameter
K_r	PPM radius scaling parameter
ℓ	PPM actuator proof-mass coordinate
L	PPM actuator characteristic length
L_n	left eigenvector corresponding to n^{th} eigenvalue
L_s	uniform beam length
m	modal index for rectangular plate
m	mass of actuator proof-mass
m_i	i^{th} modal index for rectangular plate
M	rectangular plate mass
M_s	uniform beam mass
p	passive control gain of generic damping actuator
p_a	passive control gain of a^{th} damping actuator
p'	passive contribution to damping

q	ratio of roll-off time constants
q_o	ratio of passive to active damper time constants
r	sensor index
r	radius of PPM actuator electrodynamic motor
r	rectangular plate aspect ratio
R_n	right eigenvector corresponding to n^{th} eigenvalue
R	ratio of active-to-passive damping
R_{max}	maximum value of R ensuring robustness
s	Laplace Transform variable
S	matrix constructed with the mode shapes for LAC synthesis
S_{ni}	element of S
T	PPM actuator torque output
u	input vector
v	PPM actuator velocity
W	root shift weighting matrix for LAC synthesis
W_R	modal weights
x	abcissa of a point on the rectangular plate
x	relative displacement of the actuator proof-mass
X	normalized abcissa of a point on the rectangular plate
X_a	normalized abcissa of a^{th} actuator on the rectangular plate
X_r	normalized abcissa of r^{th} sensor on the rectangular plate
y	ordinate of a point on the rectangular plate
y	measurement vector
y	inertial displacement of a point of a structure
Y	normalized ordinate of a point on the rectangular plate
Y_a	normalized ordinate of a^{th} actuator on the rectangular plate
Y_r	normalized ordinate of r^{th} sensor on the rectangular plate

z	filter state vector
z	vertical displacement of a point of the rectangular plate
z_i	vertical displacement of the i^{th} rectangular plate mode
z_{mn}	vertical displacement of the (m,n) rectangular plate mode
Z	function of active and passive roll-off time constants.
β_n	n^{th} root of the beam frequency equation
δ_{ij}	Kronecker symbol
ϕ_n	structure n^{th} real mode shape vector
ϕ_{an}	mode shape amplitude at a^{th} actuator
ϕ_{rn}	mode shape amplitude at r^{th} sensor
ϕ_n^A	n^{th} complex "actuator mode shape" vector
ϕ_n^R	nth complex "sensor mode shape" vector
ϕ_{an}^A	component of ϕ_n^A at a^{th} actuator
ϕ_{rn}^R	component of ϕ_n^R at r^{th} sensor
ζ	generic damping ratio
ζ_c	active damping ratio
ζ_n	damping ratio of n^{th} mode
ζ_p	passive damping ratio
λ_n	n^{th} eigenvalue, root
Θ	proof-mass actuator angular travel
Θ_m	maximum Θ

τ	time-constant
$1/\tau_1$, $1/\tau_2$	poles of active LAC damper
$1/\tau_o$	pole of passive LAC damper
ρ	surface mass-density of rectangular plate
ω_n	n^{th} frequency

LOW-AUTHORITY CONTROL (LAC) FOR STRUCTURES

Generalized Low Authority Control (LAC) Theory

The LAC theory originally developed for uncontrolled and undamped structures Refs. [2] and [3]. may be generalized to any linear time-invariant system of the form:

$$\left.\begin{aligned} \dot{X} &= FX + Gu \\ y &= HX \\ \dot{z} &= Az + By \\ u &= Cz \end{aligned}\right\} \qquad (1)$$

where X is the state vector $[\dot{q}\ q]^T$ (q: modal amplitudes), u the control vector, y the measurement vector, z the filter state vector, and F, G, H, A, B, and C are constant coefficient matrices. In this formulation, the z equation (filter) may be used to model either sensor dynamics (in which case z is the actual sensor output), actuator dynamics (in which case z is the actual force/torque output), any type of linear filtering including state estimators (in which case z is an estimate of the state X), or any combination of the above.

There are two reasons for extending the LAC theory to these more general systems:

(1) The introduction of the general matrices F and G (representing the dynamics of the system) allows the handling of structures which already have some natural damping or some embedded attitude or structural control systems. As will be seen subsequently, such generalization of LAC will make it possible to develop a sequential algorithm for the control synthesis.

(2) The introduction of a "filter" equation provides a convenient way to model sensor or actuator dynamics or controller roll-off, and has led to a very important result concerning the stability of real-life active LAC dampers.

It will be shown that when the general LAC formulas are applied to undamped, open-loop structures, they reduce to the simpler forms obtained directly in previous studies (Refs. [1] and [2]).

In order to apply the perturbation theory, the matrix C (or B) in (1) is assumed to be "small" in some sense, so that the shift in the n^{th} root of the open-loop system will be (shown to be) given by

$$d\lambda_n \cong -\frac{1}{2} \sum_{a,r} D_{arn} \phi^A_{an} \phi^R_{rn} \tag{2}$$

where D_{arn} is the $(a,r)^{th}$ element of the matrix

$$D_n \equiv C (A - \lambda_n I)^{-1} B \tag{3}$$

and ϕ^A_{an} and ϕ^R_{rn} are respectively the a^{th} and r^{th} components of the generalized actuator and sensor mode-shape vectors given by

$$\phi^A_n \equiv G^T L_n \tag{4}$$

$$\phi^R_n \equiv H R_n \tag{5}$$

where L_n and R_n are, respectively, the left and right eigenvectors of F corresponding to the n^{th} root λ_n of F.

Since eigenvectors are only defined to within a (complex) scalar multiplicative constant, defintions (4) and (5) depend upon the choice of separate normalizations for L_n and R_n. However, Eq. (2) is valid for <u>any</u> normalization of these vectors as long as, together, they satisfy the condition $L_n^T R_n = 2$. This particular choice is made so that Eq. (2) be formally compatible with Eq. (16) of Ref. [2] and Eq. (27) of Ref. [3].

The indices a,r in Eq. (2) refer, respectively, to the a^{th} input u_a controlling the system of actuators and the r^{th} measurement y_r of the system of sensors.* In simple cases, the indices a and r may be directly associated with (respectively) single-degree-of-freedom actuators and sensors. In more general cases, however, a single input u_a may drive several actuators, and/or a single measurement y_r may be a linear combination of several sensor outputs.

The derivation of Eq. (2) proceeds from first rewriting Eq. (1) as the single matrix equation

$$\begin{bmatrix} \dot{X} \\ z \end{bmatrix} = \left[\begin{array}{c|c} F & GC \\ \hline BH & A \end{array}\right] \begin{bmatrix} X \\ z \end{bmatrix} \tag{6}$$

and considering the open-loop (unperturbed) matrix

$$\mathcal{A} \equiv \left[\begin{array}{c|c} F & O \\ \hline BH & A \end{array}\right] \tag{7}$$

and the perturbation

$$d\mathcal{A} \equiv \left[\begin{array}{c|c} O & GC \\ \hline O & O \end{array}\right] \tag{8}$$

In order to apply Jacobi's formula (Refs. [1] or [2], Eq. (5)) the right and left eigenvectors $\mathcal{R}_n$ and $\mathcal{L}_n$ of $\mathcal{A}$ are needed. As can be easily verified,

*The suffix "s" for sensor is not used in order to avoid confusion with the common usage of s in Laplace transforms.

these are

$$\mathcal{R}_n = \begin{bmatrix} R_n \\ \hline R'_n \end{bmatrix} \tag{9}$$

$$\mathcal{L}_n = \begin{bmatrix} L_n \\ \hline O \end{bmatrix} \tag{10}$$

where

$$R'_n \equiv -(A - \lambda_n I)^{-1} BHR_n \tag{11}$$

Jacobi's formula is then written as

$$d\lambda_n = \begin{bmatrix} L_n^T & O \end{bmatrix} \left[\begin{array}{c|c} O & GC \\ \hline O & O \end{array}\right] \begin{bmatrix} R_n \\ \hline R'_n \end{bmatrix} \tag{12}$$

or

$$d\lambda_n = -L_n^T GC (A - \lambda_n I)^{-1} BH R_n \tag{13}$$

which leads to Eq. (2) when the definitions (3), (4), and (5) are used.

It is interesting now to apply Eq. (2) to an undamped, uncontrolled structure, for the case where

(i) Sensors and actuators are physically colocated*

(ii) Sensors and actuators are consistent, i.e., are of corresponding types: translation/force, rotation/torque

(iii) Sensors measure rates

---

*This does not necessarily require that the sensor-to-actuator feedback is also colocated.

In that case, we have

$$\left.\begin{aligned} H &= [\Phi \,\vdots\, 0] \\ G^T &= [\Phi \,\vdots\, 0] \end{aligned}\right\} \tag{14}$$

where Φ is the matrix of (real) structural mode shapes ϕ_n. In addition, if we normalize the eigenvectors L_n and R_n so that (compare to Eq. (11) of Ref. [2])

$$\left.\begin{aligned} R_n &= [0\ 0 \ldots 0\ 1\ 0 \ldots 0 \,\vdots\, 0\ 0 \ldots 0 \ldots 1/i\omega_n\ 0 \ldots 0]^T \\ L_n &= [0\ 0 \ldots 0\ 1\ 0 \ldots 0 \,\vdots\, 0\ 0 \ldots 0 \ldots i\omega_n\ 0 \ldots 0]^T \end{aligned}\right\} \tag{15}$$

(for which $L_n^T R_n = 2$, as required), then Eqs. (4) and (5) reduce to

$$\left.\begin{aligned} \phi_{an}^A &= \phi_{an} \\ \phi_{rn}^R &= \phi_{rn} \end{aligned}\right\} \tag{16}$$

so that Eq. (2) becomes the quadratic form

$$d\lambda_n \cong -\frac{1}{2} \sum_{a,r} D_{arn}\, \phi_{an}\, \phi_{rn} \tag{17}$$

The above formula is very similar to Eq. (16) of Ref. [1], but the filter [third equation in Eq. (1)] introduces two main differences:

(1) The coefficients $D_{arn} = D_{ar}(n)$ now depend upon the mode number n
(2) They are now complex quantities so that, in general, the $d\lambda$'s are also complex, i.e., first-order shift in frequencies may be obtained along with damping.

When the eigenvalues of the filter (i.e., the eigenvalues of A) become large compared to those of the structure, Eq. (3) shows that D_{arn} becomes independent of n and thus Eq. (17) converges to the old Eq. (16) of Ref. [1] and corresponds to the reduced equations

$$\left.\begin{aligned} &\text{Dynamics:} && \dot{X} = FX + Gu \\ &\text{Sensors:} && y = HX \\ &\text{Controls:} && u = -Dy \end{aligned}\right\} \tag{18}$$

The above equations, along with definitions (4) and (5) for generalized actuator and sensor modes, and the revised Eq. (17) for large filter eigenvalues (large filter bandwidth), i.e.,

$$d\lambda_n \equiv -\frac{1}{2}\sum_{a,r} D_{ar}\,\phi^A_{an}\,\phi^R_{rn} \tag{19}$$

are a convenient set to use when sensor, actuator, or filter dynamics can be ignored or are already embedded in the system. Indeed, in this latter case, using the definition (6) for $\mathcal{A}$, Eq. (1) can be rewritten as

$$\begin{bmatrix} \dot{X} \\ \cdots \\ z \end{bmatrix} = \mathcal{A}\begin{bmatrix} X \\ \cdots \\ z \end{bmatrix} + \begin{bmatrix} G \\ \cdots \\ O \end{bmatrix} u$$

$$y = [O : 1]\begin{bmatrix} X \\ \cdots \\ z \end{bmatrix} \tag{20}$$

$$u = Cy$$

which has the same form as Eq. (18). Equations (18) and (19) are the basis for the general LAC synthesis (LACSYS) procedure and its iterative verson (sequential LACSYS), which are discussed in the next section.

Low Authority Control Synthesis (LACSYS)*

Equation (19) of the previous section is the basic LAC prediction formula for the root shifts (hence closed-loop damping) produced by sufficiently "small" control (damping) gains D_{ar}. To synthesize the gains D_{ar}, let $(d\lambda_n)_p$ denote the predicted root shifts given by the above formula, i.e.,

$$\left.\begin{aligned}(d\lambda_n)_p &= -\frac{1}{2}\sum_{a,r} D_{ar}\,\phi^A_{an}\,\phi^R_{rn} \\ &= \text{function } (D_{ar}\text{'s})\end{aligned}\right\} \qquad (19a)$$

and let $(d\lambda_n)_D$ (given numbers) denote the desired root shifts imposed by the LAC controller design. Then the gains D_{ar} are chosen so as to minimize the weighted quadratic cost function

$$J(D) \equiv \sum_n W_n \left[(d\lambda_n)_p - (d\lambda_n)_D\right]^2 + \sum_{a,r} D^2_{ar} \qquad (20)$$

in which the modal weights W_n help specify pole locations, and the term $\sum_{a,r} D^2_{ar}$ improves robustness** of the controller, as will be shown later. Since the cost function $J(D)$ is quadratic in $(d\lambda_n)_p$ and hence, because of Eq. (19a), also quadratic in the elements of D, the gains can be obtained algebraically by solving the linear equations

$$"\frac{\partial J(D)}{\partial D} = 0" \qquad (21)$$

for (the elements of) D.

---

*The material in this section is a continuation and elaboration of the short section on Damper Design and System Robustness appearing on p. 21 of Ref. [1].

**Robustness is that quality of a controller of remaining stable in the presence of parameter variations in the structure and/or control system parameters. For instance, a stability condition independent of mode shapes and frequencies, such as the negativity of all root shifts in the fundamental LAC formula, is an expression of robustness.

To carry out this procedure, the double-indexed gain matrix D_{ar} is relabeled as a singly indexed gain vector d_i and the multiply indexed (generalized) modal coefficients ϕ^A_{an} ϕ^R_{rn} are relabeled as a coefficient matrix S_{ni}, using the same correspondence between the single index i and the pair of indices a,r, used above. The single-index relabeling scheme $(a,r) \rightarrow i$, for actuator and sensor labels which excludes those pairs for which D_{ar} is chosen to be zero*, produces a correspondence between a,r, and i such that:

$$\left.\begin{aligned} d_i &\equiv D_{a_i r_i} \\ S_{ni} &\equiv \tfrac{1}{2}\, \phi^A_{a_i n}\, \phi^R_{r_i n} \end{aligned}\right\} \qquad (22)$$

Finally, let W denote a diagonal weighting matrix whose diagonal elements are W_n, and for simplicity, denote the desired root shifts $(d\lambda_n)_D$ by $-\zeta_n\omega_n$, considered as components of a vector $-(\zeta\omega)$.

With the above relabeling, the weighted quadratic cost function in Eq. (20) can be rewritten as

$$J(d) = \sum_n W_n \left(\sum_i S_{ni} d_i - \zeta_n \omega_n \right)^2 + \sum_i d_i d_i \qquad (23)$$

or in matrix form

$$J(d) = [Sd - (\zeta\omega)]^T W [Sd - (\zeta\omega)] + d^T d \qquad (23a)$$

From Eq. (23) we can calculate the partial derivatives $\partial J/\partial d_j$ (where j is an index having the same range as i) as follows:

$$\frac{1}{2}\frac{\partial J}{\partial d_j} = \sum_n W_n \left[\sum_i S_{ni} d_i - \zeta_n \omega_n \right] S_{nj} + d_j \qquad (24)$$

*For instance, when colocated feedback is desired, $D_{ar} \equiv 0$ for $a \neq r$.

or equivalently in matrix form (I: Identity matrix)

$$\frac{1}{2}\frac{\partial J}{\partial d} = (S^T WS + I)\, d - S^T W\, (\zeta\omega) \tag{25}$$

Thus, the condition $\partial J/\partial d = 0$ leads to the LAC gain synthesis formula

$$\boxed{d = (S^T WS + I)^{-1} S^T W\, (\zeta\omega)} \tag{26}$$

In general, W is a diagonal matrix. If we assume further that the weights W_n are all equal, W becomes a scalar matrix, say $W = wI$, and Eq. (26) can then be written as

$$d = \left(S^T S + \frac{1}{w} I\right)^{-1} S^T\, (\zeta\omega)$$

so that

$$\begin{aligned} \lim_{w\to\infty} d &= (S^T S)^{-1} S^T\, (\zeta\omega) \\ &= S^{\dagger}\, (\zeta\omega) \end{aligned} \tag{27}$$

where $S^{\dagger} \equiv (S^T S)^{-1} S^T$ is the least squares pseudoinverse of S. This is the direct generalization of Eq. (18) of Ref. [2].

The purpose and effect of the term $\sum_{a,r} D_{ar}^2$ in the cost function, Eq. (20), merits further clarification. Its genesis was the purely empirical observation that, for colocated feedback, when an exact inverse solution exists (i.e., when the number of actuator/sensor pairs is equal to the number of modes to be controlled), an arbitrary specification of the desired damping ratios almost invariably leads to gains D_{aa} with large magnitude and mixed signs. In other words, the resulting control system removes energy from some parts of the structure while adding energy to other parts in order to achieve the desired (specified) modal

damping distribution. This situation is, of course, very undesirable for achieving robustness because all dampings gains must be positive to ensure unconditional stability.

It was further observed that some overall damping is always obtained by setting all the gains to some positive value of much lower magnitude, even though the resulting modal damping distribution is then quite different from the desired one. It appeared, therefore, that adding a penalty cost for large gains to the cost function J would tend to prevent the occurrence of negative gains and thus ensure robustness. This tendency can be seen directly in Eq. (26) and its limiting form, Eq. (27), for large weights. While, for large weights, nothing can be readily said concerning the sign distribution of the gains (components of the vector d), for small (positive) weights W such that W = wI we have

$$(S^T WS + I)^{-1} = I - wS^T S + \frac{1}{2} w^2 (S^T S)^2 - \ldots$$

so that Eq. (26) reduces, to first-order in w, to

$$d \cong wS^T(\zeta\omega)$$

Since, for all n, $\zeta_n \omega_n > 0$, $W_n > 0$ and the elements of S^T $\left(\text{i.e., } S_{ni} = 1/2\, \phi^2_{a_i n}\right)$ are also positive, it follows that all the gains (components of d) are also positive, and this is precisely the robustness condition which the second term in the cost function J in Eq. (20) or (23a) is intended to bring about in the LAC gain synthesis.

Remarks: In the above synthesis, the feedback (damping) gains D_{ar} were chosen to minimize the cost-function J in Eq. (20) which is the sum of two disparate design objectives: the magnitude of the errors between predicted and desired closed-loop damping, and the magnitude of the feedback gains. In this sense, an LAC system is a special case of a pareto-optimal design [1] in which multiple-objective cost functionals are optimized: the design is pareto-optimal if none of the multiple objectives can be further improved without degrading any other. While there exist

numerical techniques for multiple-objective optimization by linear programming methods using equality and inequality constraints, Ref. [4], the exact (and relatively simple) algebraic solution given by Eq. (26) is, for the case of LAC systems, a far superior synthesis method than the more general approximation techniques.

Sequential Low-Authority Control Synthesis Procedures

The low-authority controller design synthesis method discussed in the previous section is valid for a general class of linear systems, which includes, in particular, structures in which damping may be present. These systems are described in state-space form by the matrix Eqs. (18), which result in the closed-loop dynamics

$$\dot{X} = (F + GDH)X \tag{28}$$

For sufficiently "small" controls (or damping) D, written now as δD, let

$$dF \equiv G(\delta D)H \tag{29}$$

be considered as a perturbation of the dynamics matrix F consistent with the assumptions implicit in Jacobi's formula (ef. Eqs. (4), (5), of Ref. [2]. The closed-loop dynamics Eq. (28) can then be written

$$\dot{X} = (F + dF)X \tag{30}$$

The perturbation dF of the dynamics matrix introduces root shifts $d\lambda_n$ of the n^{th} (complex) root λ_n of F. When the corresponding eigenvector shifts are small, LAC theory establishes linear relationships Eq. (19) between the $d\lambda$'s and δD. Conversely, synthesis of the control gains δD corresponding to desired values of the $d\lambda$'s (or $\zeta\omega$'s) is also obtained by linear algebraic processes shown in Eq. (26) where the d's are obtained from a single-index relabeling of the doubly indexed quantities D_{ar} (now designated as small quantities δD_{ar}). However,

because of the approximations inherent to the perturbation method employed, the resultant root shifts will only approximate the desired ones.

To improve the accuracy of this process, the perturbation method is applied sequentially in a manner analogous to the Newton-Raphson method. At each step i, the small amount of control due to δD_i is "embedded" in the total dynamics, and the total system (complex) eigenvectors are recomputed. The corresponding control matrix gain increment δD_i then reduces the difference between predicted and actual closed-loop poles. This is possible because: (1) the linearity-implied additivity of the process allows one to rewrite Eq. (30) as

$$\dot{X} = [F + dF_1 + dF_2 + \ldots + dF_n]X \tag{31}$$

where

$$dF_i = G(\delta D_i)H$$

and where the corresponding final gain matrix is given by

$$D = \delta D_1 + \delta D_2 + \ldots + \delta D_n \tag{32}$$

after an n-step iteration; and Eq. (2), because of the applicability of the LAC procedure to general systems, in particular to already damped structures. A geometric interpretation of the sequential LACSYS procedure is shown in Fig. 1.

The sequential procedure is particularly useful for systems in which multiple roots occur. For such systems, the introduction of small amounts of damping generally results in large eigenvector shifts for which the LAC theory is no longer applicable. However, once a small amount of active damping has been introduced, the eigenvector indeterminacy (resulting from multiple roots) is removed, and further iterations will then make it possible to accurately synthesize the control

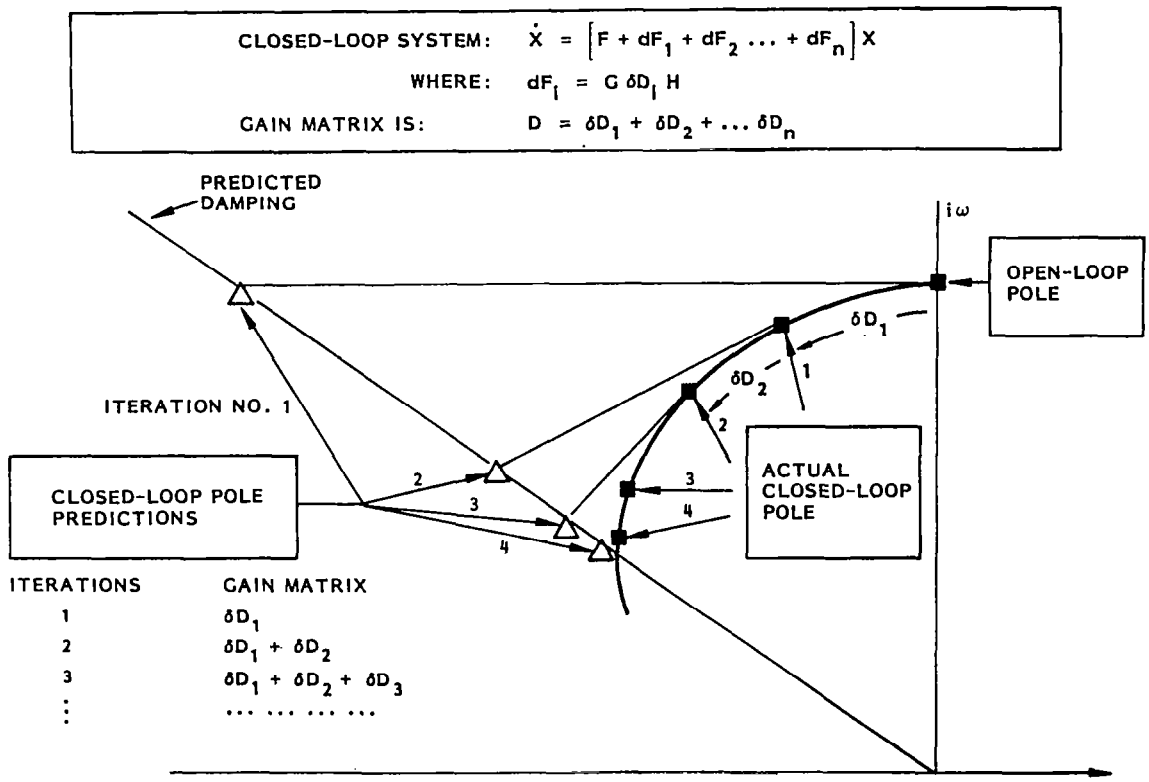

Fig. 1 Sequential Low-Authority Control Synthesis (LACSYS)

gains. This method will be applied in the sequel to illustrate an LAC design for a simply-supported rectangular plate of aspect ratio such that double-root modes occur early in the sequence of modes ordered by increasing vibration frequencies.

ROBUSTNESS* OF LAC ACTIVE DAMPERS

The generalized LAC theory makes it possible to examine various stability characteristics of idealized and incresingly more realistic systems (i.e., systems with finite bandwidth). The different cases considered lead to the final Stability Theorem for LAC active dampers in the presence of both natural structural damping and implemented passive damping.

Ideal Dampers in Undamped Structures

This case is only mentioned for completeness, since it has been largely documented in the original LAC papers Refs. [2] and [3]. Briefly summarized, for a colocated and consistent** set of actuators and sensors using rate feedback, the root shifts

$$d\lambda_n = -\zeta_n \omega_n \cong -\frac{1}{2} \sum_a D_a \phi_{an}^2 \qquad (33)$$

are always toward the left of the $i\omega$-axis for all the modes if all the gains D_a are positive. This robustness result obviously assumed that both sensors and actuators have infinite bandwidth, and also that the structure was initially undamped. Several departures from this idealization occur in actual practical cases and will be examined next.

---

*See footnote, p. 19
**See statement (ii), p. 16

Ideal Dampers in Damped Structures

Since some small amount of natural damping is usually found in any structure, or could have been already introduced by passive means, it is of interest to determine whether the addition of active dampers can still meet robustness conditions. In the case of an already damped structure for which ζ_{on} denotes the existing small damping ratio of the n^{th} mode, the dynamics matrix F in Eqs. (18) now takes the form (see Eq. (10), Ref. [3]):

$$F = \begin{bmatrix} & & \\ -2\zeta_{on}\omega_n & & -\omega_n^2 \\ & & \\ \hline & & \\ I & & 0 \\ & & \end{bmatrix} \tag{34}$$

with its eigenvalues given by:

$$\lambda_n = -\zeta_{on}\omega_n \pm i\omega_n\sqrt{1-\zeta_{on}^2} \tag{35}$$

and its right and left eigenvectors are given by $\left(\text{let } \omega_n^* \equiv \omega_n\sqrt{1-\zeta_{on}^2}\right)$:

$$\begin{aligned} R_n &= \left[0\ldots1\ldots0 \;\vdots\; 0\ldots -\left(\zeta_{on}\omega_n + i\omega_n^*\right)/\omega_n^2\ldots0\right]^T \\ L_n &= \left[0\ldots1 + i\zeta_{on}\omega_n/\omega_n^*\ldots0 \;\vdots\; 0\ldots -\omega_n^2/i\omega_n^*\ldots0\right]^T \end{aligned} \tag{36}$$

as can be verified by inspection. Note that $L_n^T R_n = 2$; see discussion below Eqs. (4) and (5). Using now Eq. (14), the generalized mode shapes Eqs. (4) and (5) for consistent sensor/actuator systems are given by

$$\left.\begin{aligned} \phi_{rn}^{R} &= \phi_{rn} \\ \phi_{an}^{A} &= \left(1 + i \frac{\zeta_{on}}{\sqrt{1-\zeta_{on}^2}}\right) \phi_{an} \end{aligned}\right\} \tag{37}$$

Thus, the real part of the root shift is

$$\mathcal{R}e(d\lambda_n) \equiv -\zeta_n \omega_n \cong -\frac{1}{2} \sum_{a,r} D_{ar} \phi_{an} \phi_{rn} \tag{38}$$

which remains always negative for colocated systems. It is to be noted, however, that in this case, there is an additional first-order shift in frequency due to the presence of the ζ_{on} term.

Actual Passive Dampers in Undamped Structures

Because of the flexibility inherent in all materials, a passive damper must be modeled at least as an ideal damper in series with a spring, as shown in Fig. 2.* As a result, the force/displacement relationship, instead of being a pure rate-feedback,

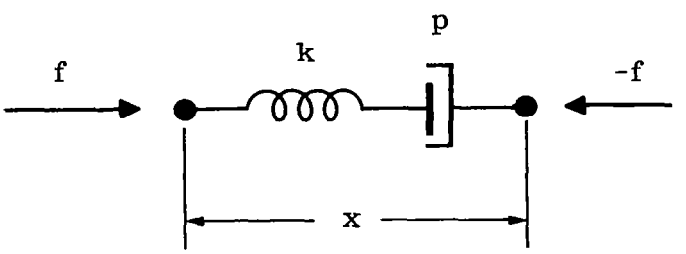

$\tau_o \equiv p/k$

Fig. 2 Passive Damper Model

*Indeed, for high frequencies, the "dashpot" part is basically locked, only the springiness of the device remains.

has a transfer function of the form

$$f(s)/x(s) = -ps/(1 + \tau_o s) \tag{39}$$

where p is the damping gain, and $\tau_o = p/k$ where k is the spring constant. This means that the actual device behaves like a pure spring rather than a damper at frequencies large compared to $1/2\pi\tau_o$. In terms of control theory, the dynamics of such devices can be represented by the first-order lag (or first-order "roll-off") $1/(1 + \tau_o s)$, placed at the output of the idealized device. Equivalently, it can be interpreted as a perfect rate-feedback system [the ps term in Eq. (39)] where the sensed rate has been "filtered" by the first-order lag filter $1/(1 + \tau_o s)$. This second interpretation is convenient for applying the generalized LAC formulas to this example. Indeed, the total system equations in this case are

$$\left.\begin{aligned} \dot{X} &= FX + Gu \\ y &= HX \\ \dot{z} &= -\frac{1}{\tau_o}(z - y) \\ u &= -pz \end{aligned}\right\} \tag{40}$$

Comparisons of Eqs. (40) with Eqs. (1) yields the corresponding Eq. (3), written for $p_a \equiv p$:

$$D_{aan} = p_a\left(\frac{1 - i\tau_o\omega_n}{1 + \tau_o^2\,\omega_n^2}\right) \tag{41}$$

and thus, for a system of passive dampers (with colocated sensing) having the same time constant τ_o, we obtain from Eq. (2)

$$\mathcal{R}e(d\lambda_n) \equiv -\zeta_{pn}\omega_n \cong -\frac{1}{2\left(1 + \tau_o^2\,\omega_n^2\right)}\sum_a p_a\,\phi_{an}^2 \tag{42}$$

which again is always negative. However, in contradistinction to the ideal damper case, the root shift now depends on the modal frequency ω_n, and the passive damping ζ_{np} becomes very small as $\tau_o \omega_n$ becomes large.

Actual Active Dampers in Undamped Structures

This is the most complicated case, but also the most interesting in terms of practical implementation of LAC systems. There are quite a number of differences between actual active dampers and the passive damper model previously described. These stem from the usually complicated dynamics of the actuator itself (e.g., nonlinearities). However, most of these unwanted characteristics can be suppressed by various methods (e.g., servo-loops around the actuator itself, electronic compensators, etc.), but one characteristic always remains, namely, the finiteness of the bandwidth. While it is reasonable to assume, for the purely passive damper, that the response $f(s)/x(s)$ for all practical purposes is not zero at very high frequency, the same assumption cannot hold in the active case where it is necessary to introduce, at the very least, another "roll-off" filter in the model.

The frequency response of such active systems will be described by the transfer function shown in Fig. 3:

$$f(s)/x(s) = \frac{cs}{(1 + \tau_1 s)(1 + \tau_2 s)} \qquad (c > o) \qquad (43)$$

where $\tau_1 \leq \tau_2$ and where c is the active control gain. For frequencies smaller than $1/2\pi\tau_1$, the system behaves like a damper, then more like a spring, and a final roll-off occurs after $1/2\pi\tau_2$ with the response going to zero with a -1 slope, as shown in Fig. 3. Unfortunately, this last roll-off may introduce enough phase shift to create instabilities if there are modes present in the roll-off region.

This problem can be treated by introducing a filter, as in the previous case.

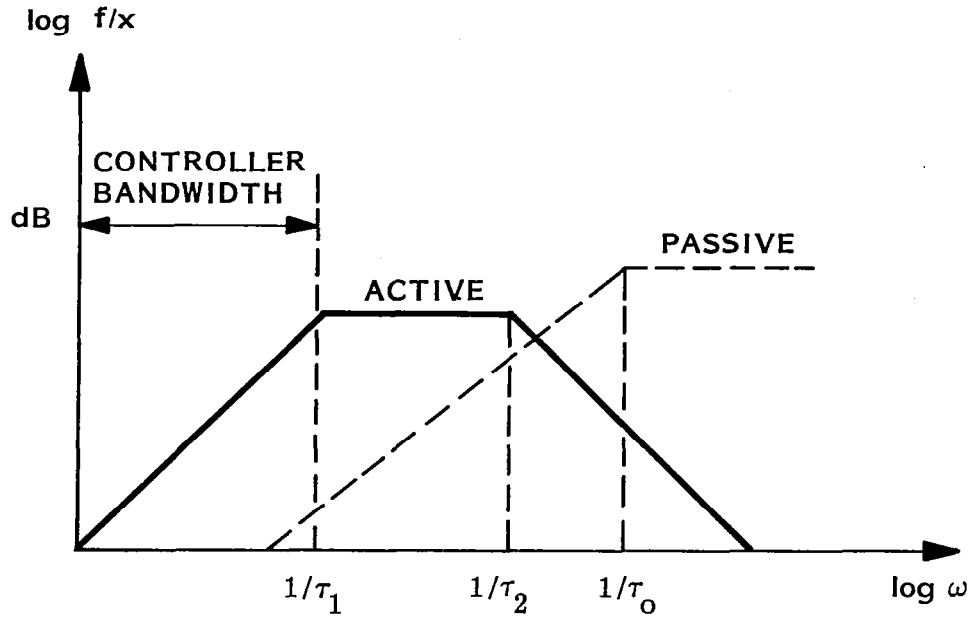

Fig. 3 Frequency Response of Active and Passive Dampers (Bode Plot)

This time the filter and control equations are

$$\begin{bmatrix} \dot{z}_1 \\ \dot{z}_2 \end{bmatrix} = \begin{bmatrix} -\frac{1}{\tau_1} & 0 \\ -\frac{1}{\tau_2} & \frac{1}{\tau_2} \end{bmatrix} \begin{bmatrix} z_1 \\ z_2 \end{bmatrix} + \begin{bmatrix} \frac{1}{\tau_1} \\ 0 \end{bmatrix} y \qquad (44)$$

$$u = \begin{bmatrix} c & | & 0 \end{bmatrix} \begin{bmatrix} z_1 \\ z_2 \end{bmatrix}$$

and application of Eq. (3) yields a result analogous to Eq. (42) for a system of identical active dampers ($c_a \equiv c$) with colocated sensing

$$\mathcal{R}e(d\lambda_n) \equiv -\zeta_{cn}\omega_n \cong -\frac{1 - \tau_1 \tau_2 \omega_n^2}{2\left(1 + \tau_1^2 \omega_n^2\right)\left(1 + \tau_2^2 \omega_n^2\right)} \sum_a c_a \varphi_{an}^2 \qquad (45)$$

This last expression for the active damping ζ_{cn} exhibits the frequency-dependent term $\left(1 - \tau_1 \tau_2 \omega_n^2\right)$ which changes sign for $\omega_n^2 > 1/\tau_1 \tau_2$. Thus, if there are any modal frequencies beyond $2\pi/\sqrt{\tau_1 \tau_2}$, the corresponding modes will always be destabilized.

This very disquieting result appears to put an end to any thought of achieving robustness or even stability in active damping of structures. But, however hopeless it may seem, it is not really serious because nature and engineering ingenuity come

to help in two ways. First, the above result is valid only for undamped structures, and will undoubtedly change if natural damping is taken into account. Second, as is graphically suggested by the curves of Fig. 3, a combined use of active and passive damping in the actuator itself could prevent this instability.*

Actual Active and Actual Passive Dampers in Damped Structures

This is the most general case, where a real structure, i.e., one which has some small amount of natural damping, is controlled by a feedback loop whose transfer function is of the type ($c > o$, $p > o$):

$$f(s)/x(s) = \frac{cs}{(1 + \tau_1 s)(1 + \tau_2 s)} + \frac{ps}{1 + \tau_o s} \qquad (46)$$

where c and p are, respectively, the active (controlled) and passive gains of the damping actuator. For instance, c can be implemented via some electrodynamic motor while the p may be realized by inherent back e.m.f. damping (produced by a low impedance power amplifier) or by an actual passive device mounted in parallel with the actuator. The time constants τ_1 and τ_2 are chosen to roll-off the active compensation well before additional poles due to actuator and amplifier dynamics are encountered.

The total real part of the root shift $\mathcal{R}e(d\lambda_n) = -\zeta_n \omega_n$ can now be obtained by summing up the contributions in the previous cases. For instance, assuming there are a number of similar actuators, with identical active and passive gains $c_a = c$ $p_a = p$, and with colocated sensing, we have:**

---

* This solution was originally proposed in 1978 by J. N. Aubrun and M. G. Lyons on the basis of root loci considerations. The ensuing stability theorem is due to Aubrun.

** The case of nonsimilar actuators is conceptually straightforward, but computationally quite involved since, for that case, τ_i ($i = 0, 1, 2$) must be replaced by τ_{ia} (actuator-dependent) and the corresponding terms can no longer be pulled out of the summation Σ_a in Eqs. (42) and (45).

$$2\zeta_n\omega_n = 2\zeta_{on}\omega_n + \sum_a \left[\frac{p_a}{\left(1+\tau_o^2\omega_n^2\right)} + \frac{1-\tau_1\tau_2\omega_n^2\ c_a}{\left(1+\tau_1^2\omega_n^2\right)\left(1+\tau_2^2\omega_n^2\right)} \right] \phi_{an}^2 \qquad (47a)$$

$$= 2\zeta_{on}\omega_n + \frac{p'}{\left(1+\tau_o^2\omega_n^2\right)} + \frac{\left(1-\tau_1\tau_2\omega_n^2\right)c'}{\left(1+\tau_1^2\omega_n^2\right)\left(1+\tau_2^2\omega_n^2\right)} \qquad (47b)$$

where
$$p' \equiv \sum_a p_a \phi_{an}^2 = p \sum_a \phi_{an}^2 \cong 2\zeta_{pn}\omega_n$$

and
$$c' \equiv \sum_a c_a \phi_{an}^2 = c \sum_a \phi_{an}^2 \cong 2\zeta_{cn}\omega_n \qquad (48)$$

The question now arises: does there exist a relation between the parameters τ_0, τ_1, τ_2, ζ_{on}, p, and c such that, when satisfied, the RHS of Eq. (47) is always positive for any ω_n? The answer is in the affirmative, and is given by an inequality which places an upper bound R_{max} on the ratio R of the active/passive LAC damping ratios $c'/[p' + 2\zeta_{on}\omega_n]$, and this in turn puts an upper bound on the achievable active damping ratio ζ_c. This inequality is characterized in the following theorem:

LAC Stability Theorem (Aubrun): Unconditional stability of an LAC system is guaranteed if and only if, for each mode n, the active damping ratio ζ_{cn} is less than a certain maximum ζ_{cn}^*. This maximum active damping ratio in any of the modes within the bandwidth of an active LAC controller is proportional to the sum of the natural structural damping ζ_{on} and the damping ζ_{pn} introduced by a passive damper mounted in parallel with the actuator. Specifically,

$$\zeta_{cn} \le \zeta_{cn}^* = R_{max}\left(\zeta_{on} + \zeta_{pn}\right)$$

where the value of the proportionality constant R_{max} is given by:

$$R_{max} \equiv \min\left(K + 2\sqrt{K},\ \tau_1\,\tau_2/\tau_o^2\right)$$

where $$K \equiv \tau_1/\tau_2 + \tau_2/\tau_1 + 2$$

and where $1/\tau_1$, $1/\tau_2$ are the poles of the active damper, and $1/\tau_o$ is the pole of the passive damper.

Proof: Conditions are sought under which the RHS of Eq. (47b) is positive for all ω_n (robustness condition). Using the following definitions:

$$\left.\begin{aligned} q &\equiv \tau_2/\tau_1 \\ q_o &\equiv \tau_o/\tau_1 \\ R &\equiv c'/\left[p' + 2\zeta_{on}\,\omega_n\left(1 + \tau_o^2\,\omega_n^2\right)\right] \\ X &\equiv \tau_1\omega_n \end{aligned}\right\} \qquad (49)$$

the robustness condition can be rewritten as

$$(1 + X^2)\,(1 + q^2X^2) + R\,(1 - qX^2)\,(1 + q_o^2\,X^2) > 0$$

which simplifies to

$$(q^2 - Rqq_o^2)\,X^4 - \left[R\,(q - q_o^2) - q_o^2 - 1\right]X^2 + R + 1 > 0 \qquad (50)$$

for all X. This is a quadratic (parabola) in the variable X^2, and a necessary condition for positivity is the positivity of the coefficient of X^4

$$R < q/q_o^2 = \tau_1\,\tau_2/\tau_o^2 \qquad (51)$$

We assume this condition can always be satisfied by the controller design. Inequality (50) will be satisfied if either of the following two conditions holds:

positivity of the coefficient of X^2, i.e.,

$$R < \frac{q + 1/q}{1 - q_o^2/q} \tag{52}$$

or negativity of the discriminant of the quadratic, i.e.,

$$R^2 - 2\frac{(q + 1/q)(1 - q_o^2/q) + 2}{(1 + q_o^2/q)^2} R + \frac{(q + 1/q)^2 - 4}{(1 + q_o^2/q)^2} < 0 \tag{53}$$

To simplify the result, it will be assumed that $q_o^2 << q$, i.e. $\tau_o^2 << \tau_1\tau_2$. In other words, the bandwidth of the passive damper is assumed to be much larger than that of the actuator. We define now

$$Z \equiv q + 1/q \tag{54}$$

and since $q_o^2/q << 1$, conditions (52) and (53) become

$$R < Z \tag{52a}$$

$$Z + 2 - 2\sqrt{Z + 2} < R < Z + 2 + 2\sqrt{Z + 2} \tag{53a}$$

The left inequality in Eq. (53a) may be ignored. Indeed, from Eq. (54) and Eq. (49) it follows that $Z = \left(\tau_1^2 + \tau_2^2\right)/\tau_1\tau_2 \geq 2$ and hence $Z + 2 - 2\sqrt{Z + 2} < Z$, so that if the left inequality in Eq. (55) were violated, it would simply be subsumed in condition (52a). Combining then inequalities (51) and (53a), the maximum value of R is chosen to be

$$R_{max} = \min\left(Z + 2 + 2\sqrt{Z + 2},\ \tau_1\tau_2/\tau_o^2\right) \tag{55}$$

Now, within the controller bandwidth, we have $\omega_n \tau_i \ll 1$, for $i = 0,1,2$. In this bandwidth, the robustness condition is thus achieved when

$$c' < R_{max} (p' + 2\zeta_{on}\omega_n) \tag{56}$$

since $R < R_{max}$, and using Eqs. (48), we finally obtain

$$\zeta_{cn} < R_{max} (\zeta_{on} + \zeta_{pn})$$

as was to be shown.

Note. In the statement of the theorem, $Z + 2$ is denoted by K. The expression $K + 2\sqrt{K}$ may also be written, after some manipulation, as $(1 + 1/q)(1 + \sqrt{q})^2$.

LAC ACTIVE DAMPING FOR SIMPLY-SUPPORTED RECTANGULAR PLATES

Simply-Supported (SS) Rectangular Plates

This chapter illustrates the synthesis of LAC active damping systems which was discussed at length in the last two sections of the first chapter. Because the strategy employed in any controller synthesis process is always dependent upon the characteristics of the structure to be controlled (i.e., actuator/sensor selection depends on controllability/observability, which in turn depends on structural mode shapes), it was suggested* that application of the LAC theory be made to simply-supported rectangular plates. The primary reason for this choice was that, for this class of structures and boundary conditions, there exist simple analytical expressions for both frequencies and mode shapes. This fact obviates the need for finite-element structural models and the ensuing numerical data processing which might obscure the controller synthesis process. A secondary reason for choosing simply-supported rectangular plates lies in the fact that, by proper choice of aspect ratio, double-roots can be made to occur early in the frequency-ordered sequence of modes. While there is, in fact, no unique eigenvector which corresponds to a double-root frequency but rather an eigenplane (invariant subspace of dimension 2), plate theory provides in that case two linearly independent orthogonal eigenvectors which span the corresponding eigenplane. This makes it possible to examine the continuum of mode shapes corresponding to multiple roots and, if these occur early in the sequence of modes, to address the actuator/sensor location problem accordingly in a reasonably low-order model.

Frequencies and Mode Shapes of SS Rectangular Plates

Consider a simply-supported rectangular plate with the following parameters:

Length:	a (m)	Poisson Ratio:	ν
Width:	b (m)	Surface Density:	ρ (kg/m^2)
Thickness:	h (m)	Flexural Rigidity:	D (N-m)
Young's Modulus:	E (N/m^2)	$D = Eh^3/[12\,(1-\nu^2)]$	

*By Dr. Larry D. Pinson, NASA Langley Research Center.

and let one of its corners coincide with the origin of a rectangular coordinate system (x,y,z), as shown in Fig. 4, where a typical point of the deformed plate has coordinates x,y, and z (x,y). It is thus assumed that the deformation field is one-dimensional, i.e., all deformations occur along the z-axis.

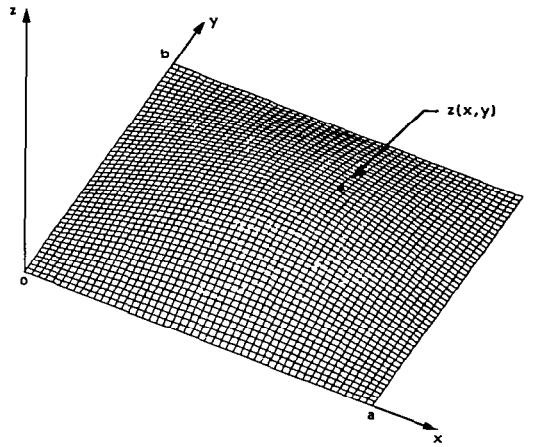

Fig. 4 Coordinates for Simply Supported Rectangular Plates

It is well-known from plate vibration theory (e.g., Ref. [5]) that the vibration frequencies of such SS-SS-SS-SS rectangular plates are given by the doubly-indexed family

$$\left.\begin{aligned} \omega_{mn} &= \sqrt{\frac{D}{\rho}}\left[\left(\frac{m\pi}{a}\right)^2 + \left(\frac{n\pi}{b}\right)^2\right] \\ &\text{(m,n: integers)} \\ &= \left(\frac{\pi}{a}\right)^2 \sqrt{\frac{D}{\rho}}\,(m^2 + r^2\, n^2) \end{aligned}\right\} \quad (57)$$

where $r \equiv a/b$ is defined as the aspect ratio of the plate. The plate deformations $z_{mn}(x,y)$ which satisfy the boundary conditions and correspond to these frequencies are given by

$$z_{mn}(x,y) = a_{mn} \sin(m\pi x/a) \sin(n\pi y/b) \quad (58)$$

where the amplitudes a_{mn} are determined from the initial conditions of the problem.

The two parameter families ω_{mn} and z_{mn} can always be linearly ordered by a single index i when the index pair (m,n) is ordered as (m_i,n_i) $(i = 1,2\ldots)$

according to some rule (e.g., increasing frequencies). Using such a correspondence $(m_i, n_i) \rightarrow (i)$, we define

$$\left.\begin{aligned} \omega_i &= \omega_{m_i n_i} \\ z_i &= z_{m_i n_i} \end{aligned}\right\} \tag{59}$$

In order that the deformation functions (or surfaces) given by Eq. (58) be mode shapes, proper normalization is required. In particular, we must then have $(i = 1,2\ldots;\ j = 1,2\ldots)$

$$\iint_{\text{Plate}} z_i(x,y)\, z_j(x,y) \rho \, dx \, dy = \delta_{ij} \tag{60}$$

which is equivalent to the standard normalization "$\Phi^T M \Phi = I$" used in structures (see Ref. [6]) where Φ is the matrix of eigenvectors (mode shapes), M is the generalized mass, and I is the identity matrix. Since the functions z_i are orthogonal, the normalization conditions of Eq. (60) reduce to

$$\rho\, a_{mn}^2 \int_0^b \int_0^a \sin^2\left(m\pi \frac{x}{a}\right) \sin^2\left(n\pi \frac{y}{b}\right) dx \, dy = 1 \tag{61}$$

which leads to (for all indices m,n)

$$a_{mn} = \sqrt{\frac{4}{\rho ab}} = \frac{2}{\sqrt{M}} \tag{62}$$

where M is the mass of the plate. Using the transformation

$$\left.\begin{aligned} X &= x/a \\ Y &= y/b \end{aligned}\right\} \tag{63}$$

the mode shapes for the plate can be written as:

$$z_{mn}(X,Y) = \frac{2}{\sqrt{M}} \sin m\pi X \sin n\pi Y \qquad x,y \in [0,1] \tag{64}$$

The affine transformation Eq. (63) maps the rectangular plate onto a square plate for any value of the aspect ratio. The surfaces $z_{mn}(X,Y)$, displayed in Fig. 5 for selected values of m, n thus represent (except for scale) the mode shapes of any rectangular plate. However, any specific ordering of the frequencies ω_{mn} (and corresponding mode shapes z_{mn}) can only be obtained by specifying first an aspect ratio r in Eq. (57).

LAC Active Damping For 3:1 Aspect Ratio Plate

To illustrate LAC active damping for a plate for which (at least) 10 percent damping is required in the first five modes, with at most five colocated actuator/sensor pairs, an aspect ratio of 3:1 is chosen. The physical parameters for this plate are as follows:

a	=	3 m
b	=	1 m
h	=	1 cm
E	=	6.9×10^{10} N/m^2 (aluminum)
ρ	=	27.6 kg/m^2 for 1 cm thick
ν	=	1/3
D	=	$Eh^3/[12(1-\nu^2)] = 6.46875 \times 10^3$ Nm
$\sqrt{D/\rho}$	=	15.3093 m^2/s
M	=	ρab = 82.8 kg

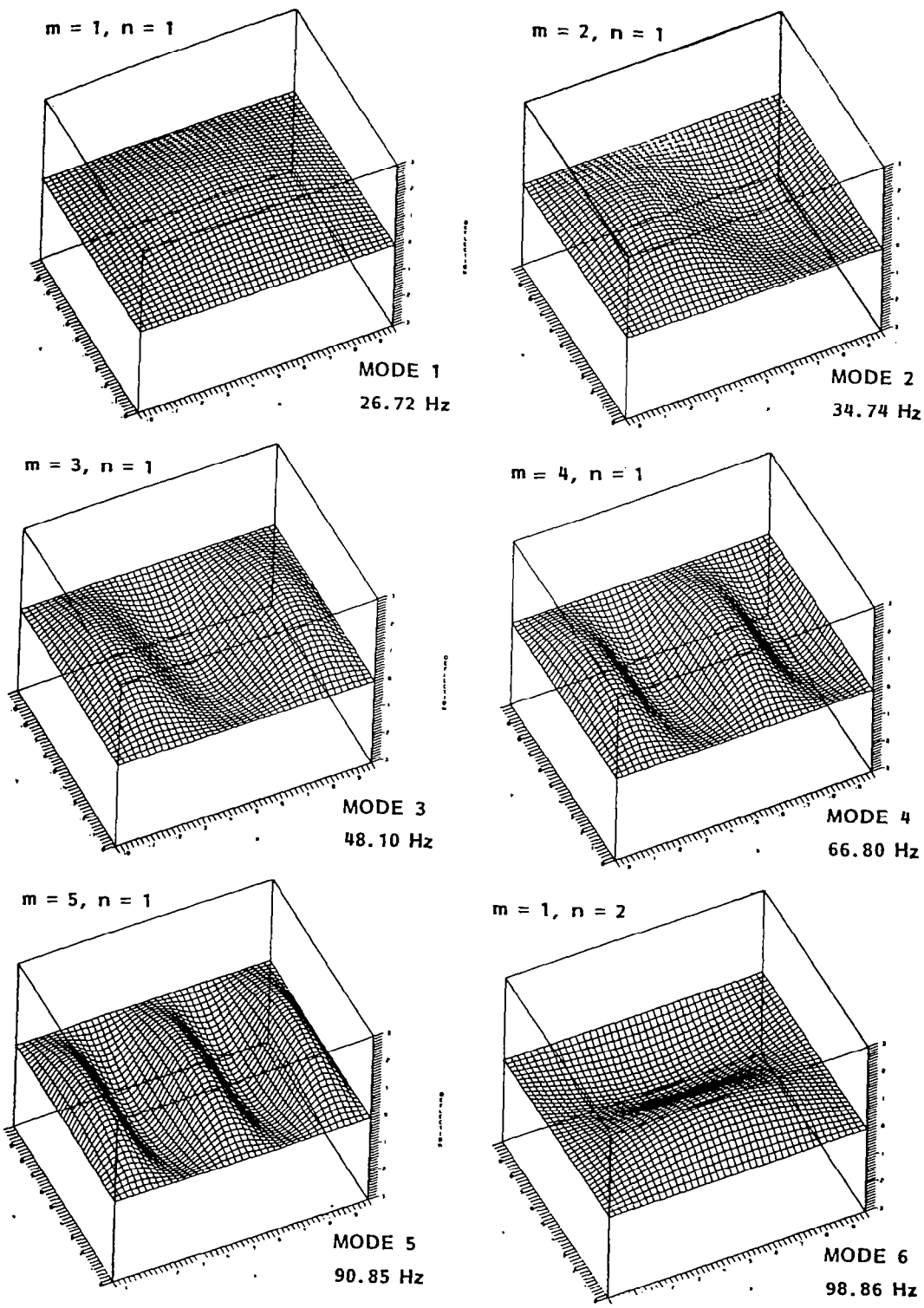

Fig. 5 Mode Shapes for Simply-Supported Rectangular Plate (3:1)

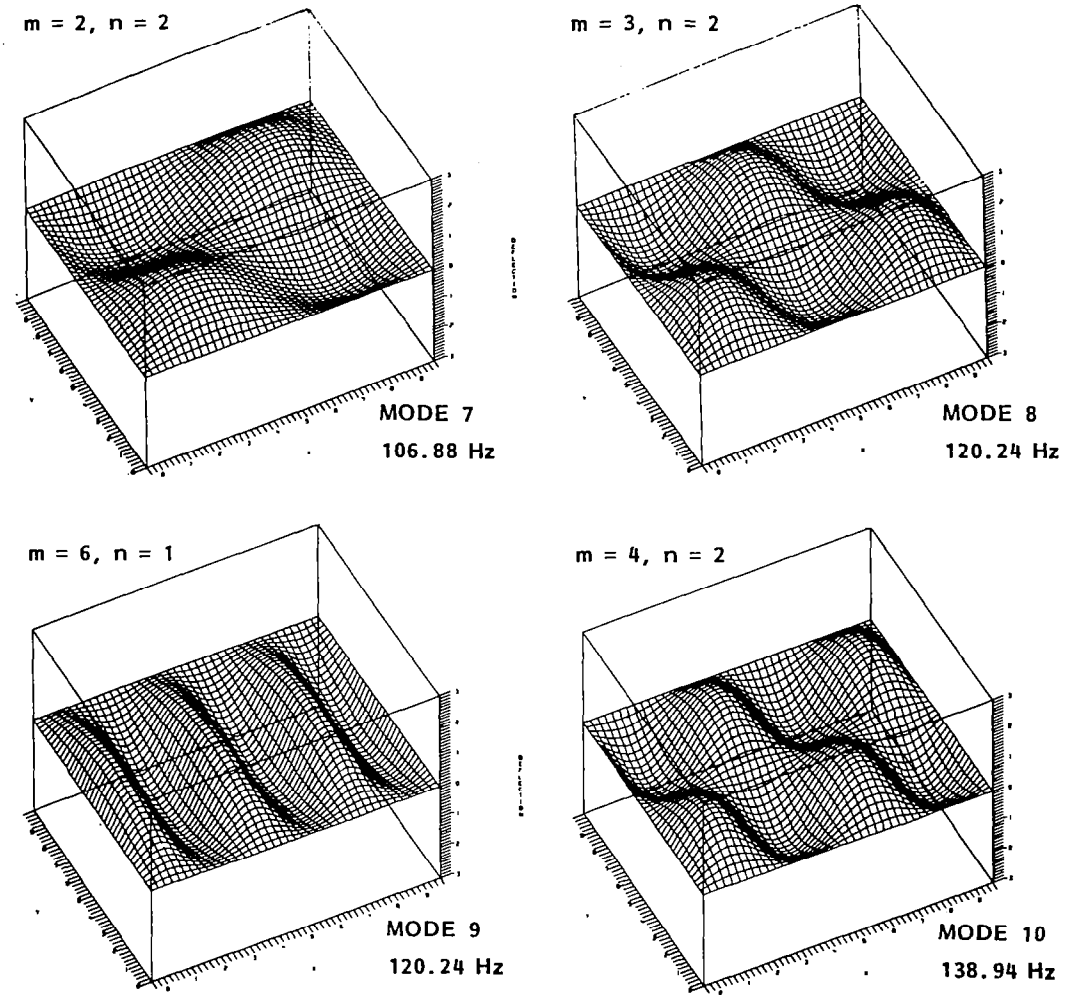

Fig. 5 (Concluded)

and its first ten modal frequencies in Eq. (57) for $r^2 = a^2/b^2 = 9$ are given by

$$\omega_i = (\pi^2/a^2)\sqrt{D/\rho}\left(m_i^2 + 9\, n_i^2\right) \tag{65}$$

where the correspondence $(m_i, n_i) \rightarrow (i)$ is obtained as follows:

Table 1. FREQUENCIES FOR 3:1 ASPECT-RATIO PLATE

Mode No. i	m_i	n_i	$\left(m_i^2 + 9\, n_i^2\right)$	$\omega_i/2\pi$ (Hz)
1	1	1	10	26.7
2	2	1	13	34.7
3	3	1	18	48.1
4	4	1	25	66.8
5	5	1	34	90.8
6	1	2	37	98.9
7	2	2	40	106.9
→ 8	3	2	45	120.2 ← } Double Root
→ 9	6	1	45	120.2 ← }
10	4	2	52	138.9

The choice of actuator/sensor locations is based on the locations of maximum modal deflection amplitudes of the plate, as shown by the modal controllability surfaces of Fig. 6. In J. N. Aubrun's Low Authority Control Theory, these arise from the fundamental root shift formula (e.g., Eq. (16), Ref. [1]) for undamped structures.

$$d\lambda_n \cong -\frac{1}{2} \sum_{a,r} D_{ar}\, \phi_{an}\, \phi_{rn} \tag{66}$$

where the coefficients D_{ar} are the damping (control) gains, with the indices a,r denoting, respectively, actuator and sensor locations on the plate so that

$$\phi_{an} \equiv z_n (X_a, Y_a)$$
$$\phi_{rn} \equiv z_n (X_r, Y_r)$$

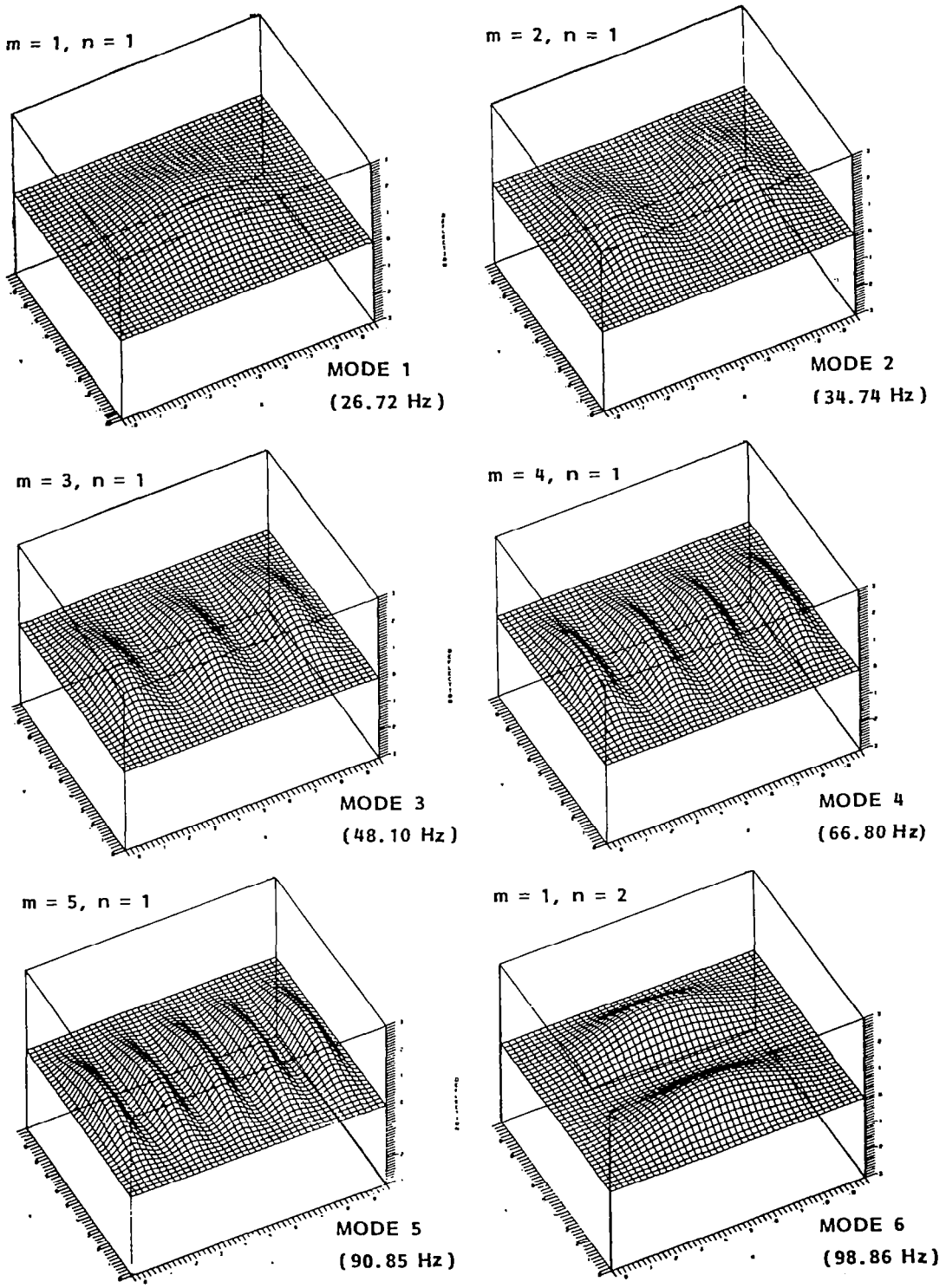

Fig. 6 Modal Controllability Surfaces for Simple-Supported Rectangular Plate (3:1)

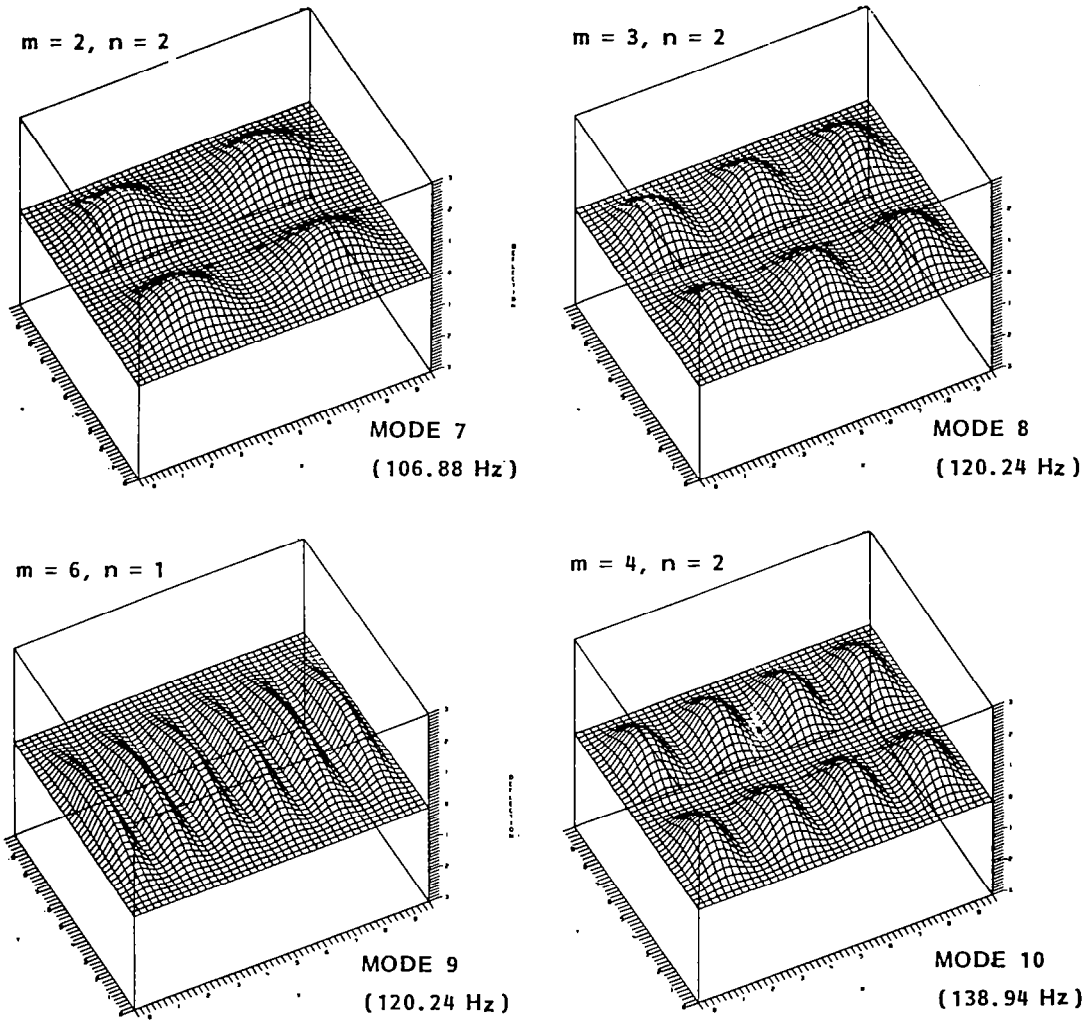

Fig. 6 (Concluded)

for each vibration mode n. For a single colocated actuator/sensor (a = r), the r.h.s. of Eq. (66) becomes $D_{aa}\,(\phi_{an})^2$, and for a given root shift, the gain D_{aa} is minimum when $(\phi_{an})^2 = [z_n\,(X_a, Y_a)]^2$ is maximum. Thus, when the actuator location (X_a, Y_a) is varied continuously over the plate, the correspondence $(\phi_{an})^2_a \rightarrow z_n^2\,(X,Y)$ generates a surface whose peaks represent optimum actuator locations for minimum gain D_{aa} for each mode n. These

controllability surfaces are thus the "squares" of the mode shapes, and are shown in Fig. 6. Figure 7 shows five actuators placed very close to the plate's

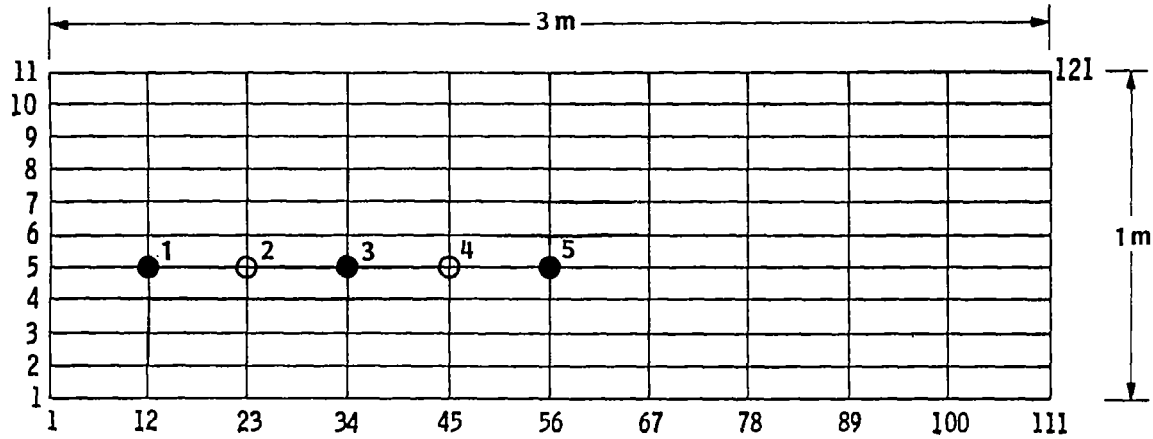

Fig. 7 Actuator Locations on 3:1 Aspect-Ratio SS-Plate

centerline Y = 1/2. The choice of these actuator locations is heuristic, and represents a compromise between exact placement on controllability peaks and available grid locations on the plate when a computationally tractable mesh size is used for the plate, e.g., 121 possible locations for actuator stations, as shown in Fig. 7. In general, one may tabulate the values of $(\phi_{an})^2$ versus a and n, and examine the ensuing matrix for its largest entries. In the present case, examination of Fig. 8 reveals directly which actuators are most (or equally most) efficient for the first five plate modes.

This matrix suggests that actuators No. 2 and No. 4 may be superfluous for damping the first five modes and this is indeed confirmed by the numerical synthesis of the LAC gains obtained by Eq. (26) of the LACSYS procedure.

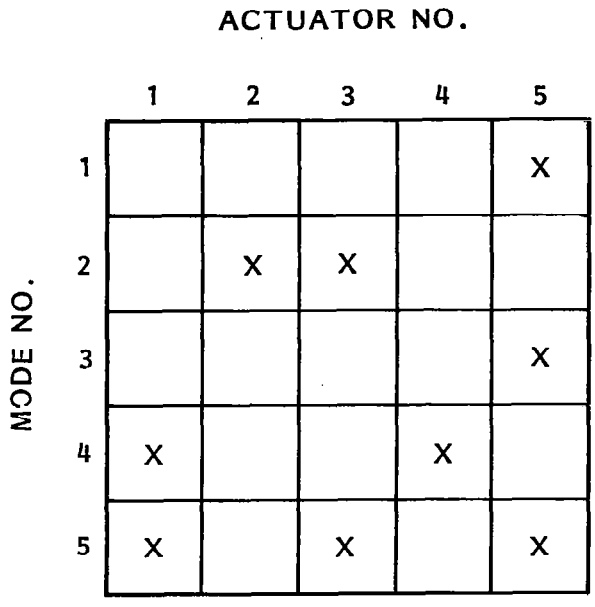

Fig. 8 Actuator Effectiveness Matrix for 3:1 Aspect-Ratio Plate

Table 2 gives results of this synthesis for all five actuators.

Table 2 LAC SYNTHESIS FOR FIVE ACTUATORS

Mode No.	OPEN-LOOP Freq. (Hz)	LACSYS Weights	LAC PREDICTED CLOSED-LOOP Freq. (Hz)	LAC PREDICTED CLOSED-LOOP Damping (%)	FULL EIGENANALYSIS CLOSED-LOOP Freq. (Hz)	FULL EIGENANALYSIS CLOSED-LOOP Damping (%)	
1	26.7	7.50	26.9	11.0	27.7	10.31	CONTROL DESIGN
2	34.7	0.75	35.0	11.5	34.7	12.09	
3	48.1	7.50	48.4	10.9	48.7	11.27	
4	66.8	0.90	67.1	10.0	68.2	11.02	
5	90.8	0.75	91.3	10.0	88.9	11.92	
6	98.9	0	98.9	1.1	98.8	1.13	SPILLOVER
7	106.9	0	106.9	1.4	106.6	1.43	
8	120.2	0	120.2	1.4	116.3	5.52	
9	120.2	0	120.2	1.4	120.2	0.63	
10	138.9	0	138.9	1.8	137.7	1.09	

The gains obtained with the above are (let $D_{aa} \equiv D_a$):

$$\left.\begin{aligned} D_1 &= 1{,}830.0 \ \text{N-s/m} \\ D_2 &= 1.9 \ \text{N-s/m} \\ D_3 &= 544.0 \ \text{N-s/m} \\ D_4 &= 86.1 \ \text{N-s/m} \\ D_5 &= 238.0 \ \text{N-s/m} \end{aligned}\right\} \qquad (67)$$

so that $\sum_a |D_a| = 2{,}700$ kg/s. The gains D_2 and D_4 thus contribute relatively very little to the control effort, and removing actuators No. 2 and No. 4 yields the following results for the final closed-loop eigenanalysis:

Table 3 CLOSED-LOOP FREQUENCIES AND DAMPING FOR ACTUATORS NO. 1, 3, AND 5

Mode No.	Closed-Loop Freq. (Hz)	Damping (%)
1	27.49	10.51
2	34.99	10.58
3	48.58	12.02
4	68.04	10.03
5	89.07	12.05

with control gains

$$\left.\begin{aligned} D_1 &= 1{,}798.0 \ \text{N-s/m} \\ D_3 &= 486.0 \ \text{N-s/m} \\ D_5 &= 350.0 \ \text{N-s/m} \end{aligned}\right\} \qquad (68)$$

for which a measure of the control effort is $\sum_a |D_a| = 2{,}635$ kg/s.

Remarks: (A) The desired modal dampings in $(\zeta\omega)$ of the LACSYS Eq. (26) used in the above synthesis procedure were 11 percent for the first five modes, and 0 for the remaining ones. The intent was to achieve at least 10 percent damping in the first five modes only, so no attempt was made to control the other ones. (This was already evident in the choice* of actuator/sensor locations which were such that modes Nos. 6, 7, 8, and 10 were essentially unobservable and uncontrollable, i.e., $\phi_{an} = \phi_{rn} \sim 0$ since the centerline $Y = 1/2$ is a nodal line for all these modes.) This restriction to the first five modes is quite arbitrary, and any number of modes could have been selected providing sufficiently many actuators are used. Indeed, it has been previously shown (p. 21, Ref. [1]) that in order to specify the damping ratio of N_c structural modes, N_c colocated sensor/actuator damping units are required. The fact that it is possible to use fewer than five actuators for the SS plate cannot be generalized to arbitrary structures; whether or not one may use fewer than N_c units in the general case depends on the mode shape configurations.

(B) Modes Nos. 8 and 9 correspond to a double root for which, strictly speaking, there is no (unique) associated eigenvector but rather an "eigenplane" in modal space. That is, any (pointwise) linear combination of the surfaces $z_8(X,Y)$ and $z_9(X,Y)$ is again a mode shape surface corresponding to the double root $\omega_8 = \omega_9$ at 120.24 Hz, and as an example, Figs. 9(a) and 9(b) illustrate the surfaces $z_8 + z_9$ and $z_8 - z_9$, both of which are also vibration modes at that same frequency. The special difficulty with multiple root modes is that the presence of an actuator on one of their controllability surface peaks cannot guarantee any kind of damping performance because the vibration pattern simply shifts around so that the controllability peak reemerges elsewhere, away from the actuator, as can be seen in Figs. 9(a) and 9(b). From a mathematical point of view, the LAC perturbation theory no longer applies because a small root shift can produce a very

*The five actuators were placed slightly "below" the plate's horizontal centerline, by a distance equal to 1/10 of the plate's width, as shown in Fig. 7. The idea was to create a very small spillover into modes Nos. 6, 7, 8, and 10 without any attempt to control them. In practice, actuator-mounting errors and resulting spillover will always occur.

large eigenvector shift. The method devised to deal with multiple root modes is a consequence of the sequential LACSYS procedure and is discussed next.

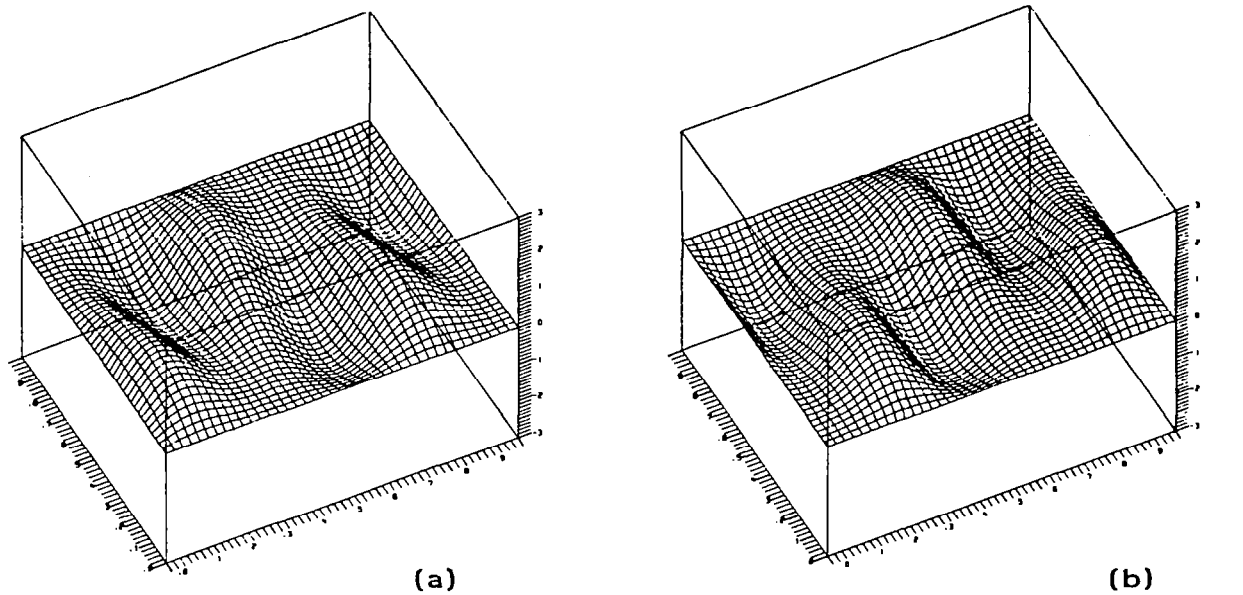

Fig. 9 Example of Alternate Mode Shapes Corresponding to Double Roots

LAC Active Damping For $\sqrt{5/3}$:1 Aspect Ratio Plate

In the previous 3:1 aspect ratio plate, modes No. 8 and 9 were double-root modes. The study of such modes (if they were to be included without omitting previous ones) would then require a relatively high-order model, e.g., of order 20 for the first 10 modes. In order to avoid higher order models, a new aspect ratio was sought such that double roots would occur last in a five-mode model. Inspection of Eq. (57) shows that this can be achieved for an aspect ratio $r = \sqrt{5/3}$ for which we obtain the frequencies shown in Table 4.

Table 4. FREQUENCIES FOR $\sqrt{5/3}$:1 ASPECT-RATIO PLATE

Mode No. i	m_i	n_i	$\left(m_i^2 + \frac{5}{3} n_i^2\right)$	$\omega_i/2\pi$ (Hz)
1	1	1	2.666...	7.125
2	2	1	5.666...	15.141
3	1	2	7.666...	20.485
→ 4	3	1	10.666...	28.501 ← } Double Root
→ 5	2	2	10.666...	28.501 ← }
6	3	2	15.666...	41.861
7	1	3	16.000...	42.752
8	4	1	17.666...	47,205

where the plate parameters are the same as before, except that now $b = 2.324$ m. The first three mode shapes and the corresponding modal controllability surfaces are shown in Fig. 10. The fourth and fifth mode shapes, given by the surfaces

$$\left.\begin{aligned} z_4(X,Y) &= 2/\sqrt{M}) \sin(3\pi X) \sin(\pi Y) \\ z_5(X,Y) &= 2/\sqrt{M}) \sin(2\pi X) \sin(2\pi Y) \end{aligned}\right\} \tag{69}$$

correspond to the double root above at 28.501 Hz. These two surfaces are orthogonal eigenvectors corresponding to the double eigenvalue $\omega_4 = \omega_5$. i.e.,

$$\iint_{\text{Unit square}} z_4(X,Y)\, z_5(X,Y) \rho \, dX \, dY = 0$$

and hence any (pointwise) linear combination of these surfaces corresponds again to an eigenvector at the same frequency. Thus, the surface $z_\theta(X,Y)$ defined by

$$z_\theta(X,Y) \equiv \cos\theta \, z_4(X,Y) + \sin\theta \, z_5(X,Y) \tag{70}$$

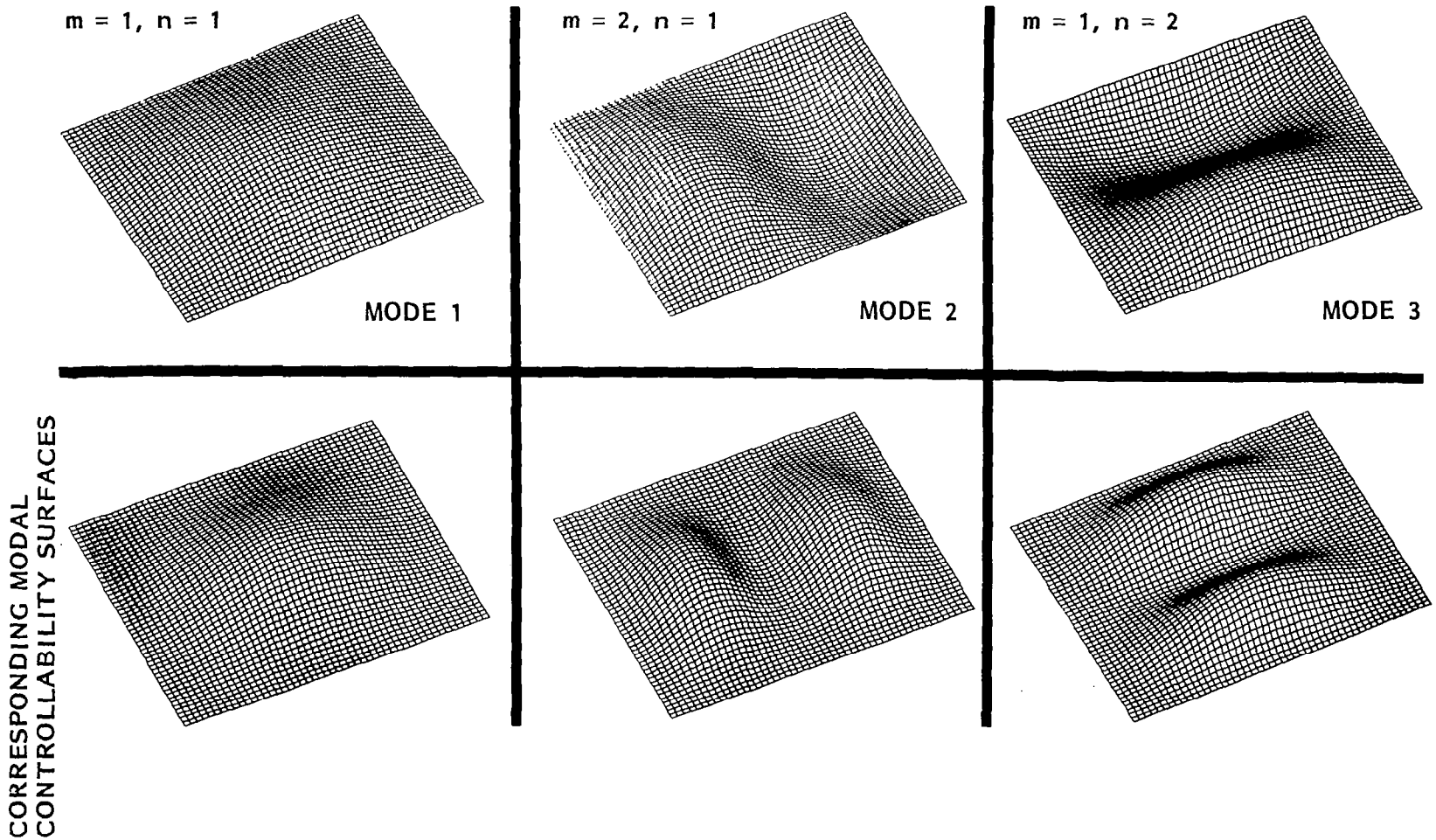

Fig. 10 First Three Mode Shapes and Modal Controllability Surfaces for $\sqrt{5/3}$:1 Aspect-Ratio SS-Plate

is also a mode shape (with the proper normalization) at that frequency. As θ varies, the one-parameter family of surfaces generated by Eq. (70) sweeps out the eigenplane corresponding to the double-root $\omega_4 = \omega_5$. Figure 11 shows a sampling of the surfaces $|z_\theta(X,Y)|$ for θ varying between 0 and $\pi/2$ in 15 deg increments, and these correspond thus to modal controllability surfaces of the continuous family Eq. (70). The peaks of these surfaces are shown in Fig. 12 (for the first five modes), together with five actuator/sensor locations chosen for this aspect-ratio plate. (See Remarks below.)

The final result of synthesizing a low-authority control damping system for the $\sqrt{5/3}$:1 aspect ratio plate is given in Table 5.

Table 5. PERFORMANCE OF LAC SYSTEM FOR $\sqrt{5/3}$:1 ASPECT-RATIO PLATE

Mode No.	Open-Loop Freq. (Hz)	(FULL EIGENANALYSIS) Closed-Loop Freq. (Hz)	Damping (%)
1	7.125	8.391	37.73
2	15.141	15.184	35.14
3	20.485	19.275	14.30
→ 4	28.501	26.800	10.43
→ 5	28.501	28.352	10.93
6	41.861	41.478	5.03
7	42.752	43.197	6.44
8	47.205	45.363	6.17

The synthesis was carried out sequentially, and the values of the weights W_n, desired damping ratios ζ_n, as well as the LAC-predicted (P) and actual (A) damping ratios occurring at each iteration of the sequential process are displayed in Table 6. The objective, as before, was to obtain at least 10 percent damping in the first five modes in a "balanced" fashion, i.e., without imposing excessively high damping in any particular mode.

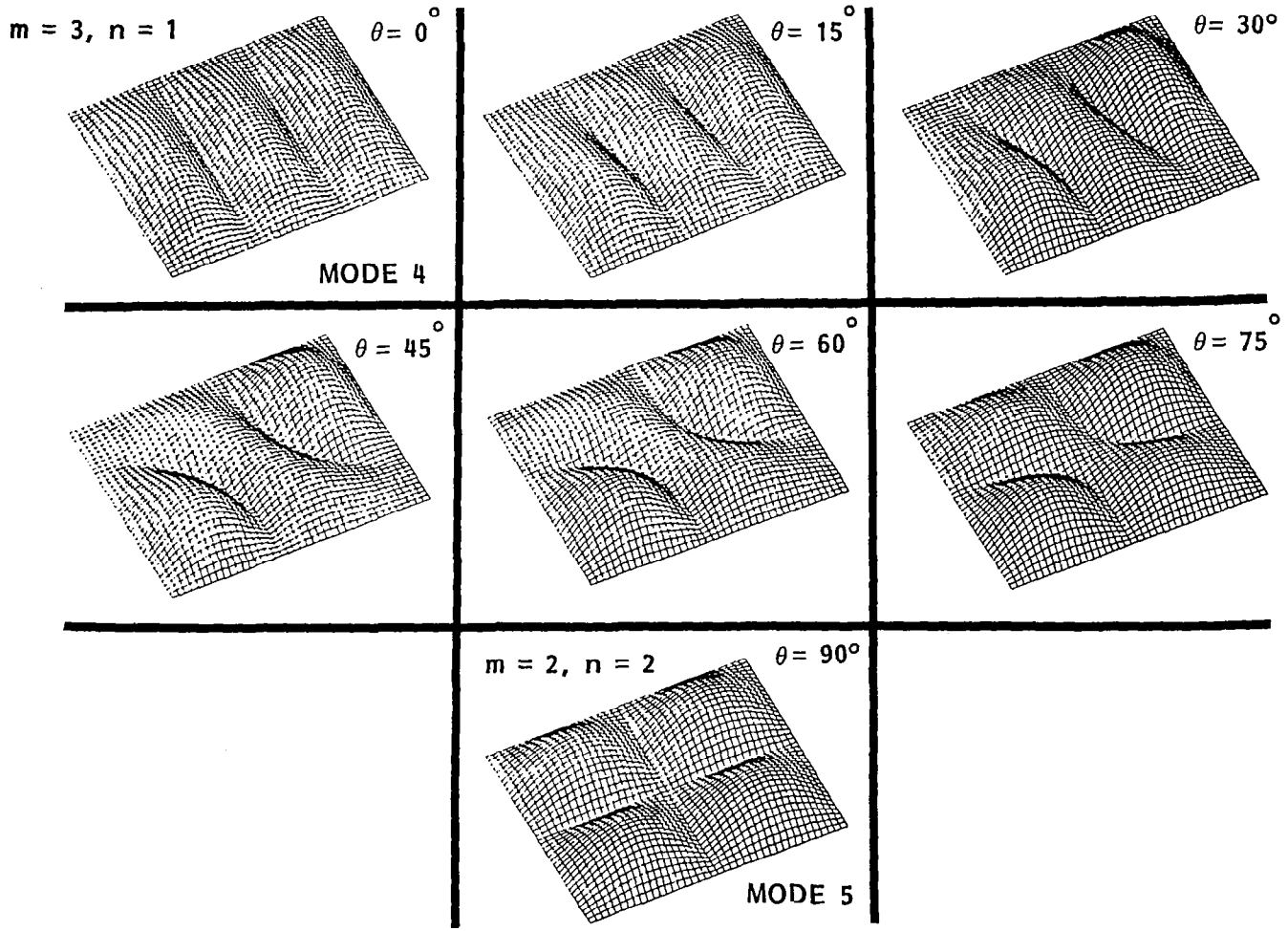

Fig. 11 Continuous Family of Modal Controllability Surfaces for $\sqrt{5/3}$:1 Aspect-Ratio SS-Plate

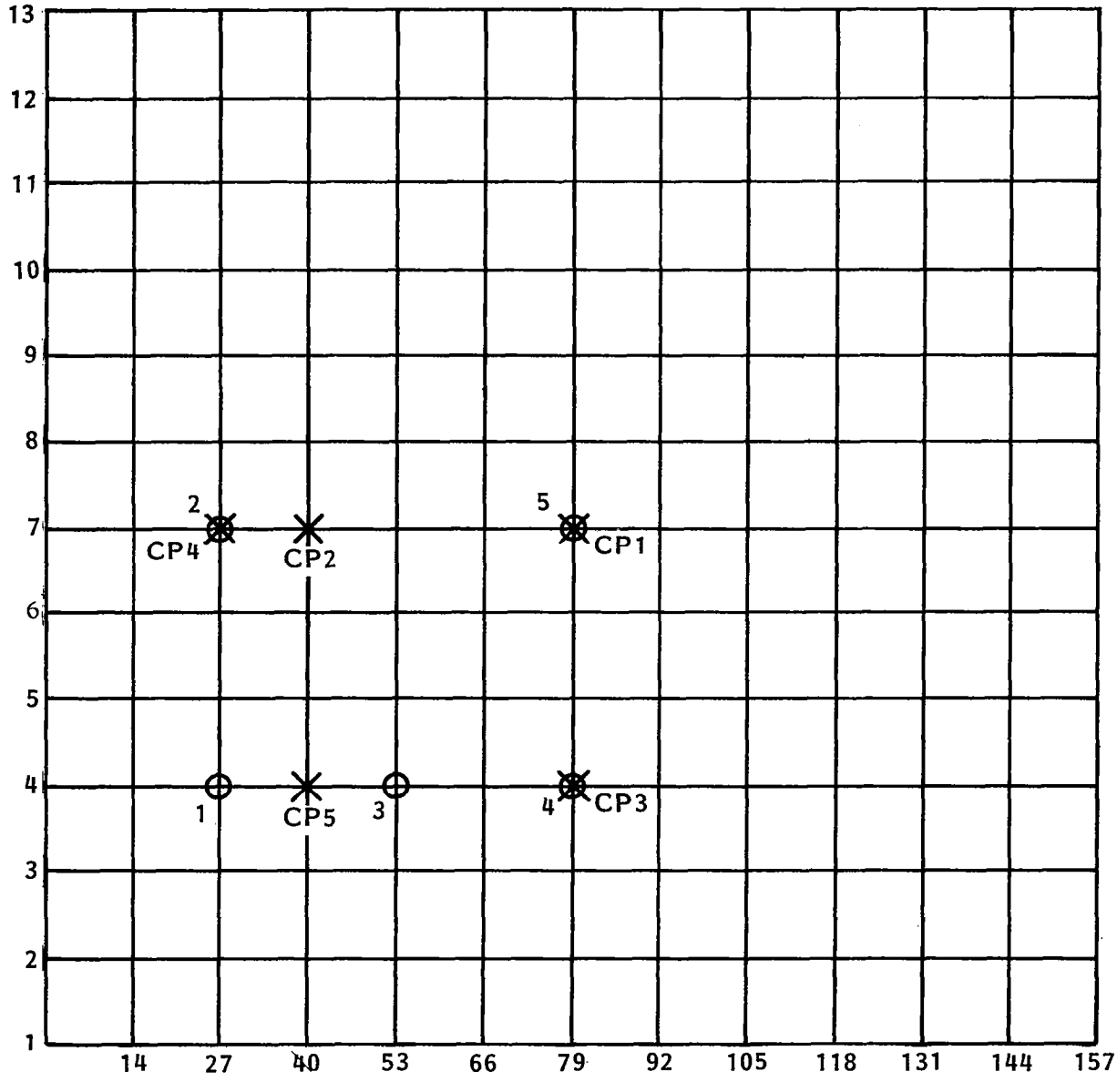

Fig. 12 Actuator Locations and Modal Controllability Peaks for $\sqrt{5/3}$:1 Aspect-Ratio SS-Plate

Table 6 SEQUENTIAL LOW-AUTHORITY CONTROL SYNTHESIS FOR $\sqrt{5/3}$:1 ASPECT-RATIO SS-PLATE

Mode No.	Open-Loop Frequency (Hz)	PERCENT CLOSED-LOOP DAMPING (P: PREDICTED BY LAC THEORY; A: ACTUAL OBTAINED BY FULL EIGENANALYSIS)																							
		Iteration 1		Iteration 2		Iteration 3		Iteration 4		Iteration 5		Iteration 6		Iteration 7		Iteration 8		Iteration 9		Iteration 10		Iteration 11		Iteration 12	
		P	A	P	A	P	A	P	A	P	A	P	A	P	A	P	A	P	A	P	A	P	A	P	A
1	7.1	6.1	6.1	20.4	21.1	22.3	–	23.6	23.5	32.0	–	39.1	39.8	35.8	34.5	43.1	43.7	42.6	42.4	31.9	–	33.3	33.7	37.5	37.7
2	15.1	4.7	4.8	13.2	13.9	13.2	–	13.7	13.0	14.1	–	16.6	14.8	21.0	25.2	28.3	27.8	32.4	32.8	30.5	–	33.8	33.8	35.2	35.1
3	20.5	4.6	4.6	9.6	9.2	10.7	–	10.9	12.6	10.5	–	10.0	11.8	16.0	16.7	16.2	16.3	15.3	15.3	15.0	–	14.3	14.2	14.3	14.3
4	28.5	4.8	4.8	9.2	10.8	9.4	–	9.6	12.7	10.3	–	9.8	5.2	9.0	10.8	11.4	9.4	11.4	11.6	11.8	–	10.3	10.4	10.5	10.4
5	28.5	4.8	1.3	5.6	4.1	6.4	–	7.0	4.4	7.0	–	9.3	14.4	11.4	8.4	10.8	12.9	11.0	10.7	8.1	–	9.8	9.7	10.9	10.9
Desired Dampings ζ in $(\zeta\omega)$ Term of LACSYS Formula (26)(1)	ζ_1	5		10		10		10		23		23		–		–		–		39		30		–	
	ζ_2	5		10		10		10		11		11		–		–		–		–		–		–	
	ζ_3	5		10		10		10		11		11		–		–		–		–		–		–	
	ζ_4	5		10		10		10		11		11		11		12		12		–		–		–	
	ζ_5	5		10		10		10		11		11		11		11		11		–		11		11	
Modal Weights W_n in LACSYS Formula (26) (Dimensionless)	W_1	1		1		0.5		0.5		1		1		0		0		0		1		1		0	
	W_2	1		1		1		1		1		1		0		0		0		0		0		0	
	W_3	1		1		1		1		1		1		0		0		0		0		0		0	
	W_4	1		1		1		1.2		1		1		1		1		1		0		0		0	
	W_5	1		1		1		1.2		1		2		1		1		1		0		1		1	
Cumulative LAC Gains(2) (N-s/m)	$\Sigma\delta D_1$	487		624		1,090		1,190		766		600		934		1,090		1,180		1,140		989		989	
	$\Sigma\delta D_2$	195		995		387		317		688		996		818		977		1,070		997		1,230		1,309	
	$\Sigma\delta D_3$	281		544		1,040		1,170		988		870		1,830		1,780		1,880		1,780		1,850		1,886	
	$\Sigma\delta D_4$	233		609		212		106		436		714		343		452		324		202		285		348	
	$\Sigma\delta D_5$	698		592		221		288		486		630		265		492		451		243		169		246	
																								Final Gains	

(1) Desired dampings ζ_n in $(\zeta\omega)$ of LACSYS formula (26) have no effect when corresponding weights W_n are set to zero.

(2) The gain indices match the actuator names (numbers) shown in Fig. 12. In that figure, an actuator located at X,Y carries the grid label X + Y -1, e.g., Actuator #1 is located at grid point No. 30.

Remarks

1) The sequential synthesis process was carried out for the first five modes only of an eight-mode model. As shown in Table 5 , the "spillover" to modes 6, 7, and 8 produces about 5 to 6 percent damping in these modes. This spillover is a strong function of the relative location of actuators and controllability peaks for the "unmodeled"modes.

2) Controllability peaks represent an optimum actuator location for given modes, but damping in those modes will also occur for nearby (nonoptimum) locations for somewhat higher actuator gains. For example, as can be seen in Fig. 12, actuator No. 2 is located at CP4 (controllability peak of mode 4) and is as near to CP2 as the finite-mesh discretization of the plate will allow. (For this plate, a discretization of 12 x 12 = 144 subplates was used, with 13 x 13 = 169 grid points, including the simply-supported boundaries, available for actuator placement.) Placing another actuator at CP2 would not only be redundant for CP4, but would provide excessive control on the plate's horizontal centerline where also actuator No. 5 is located at CP1.

3) For double-root modes, controllability peaks lose their significance because of the shifting modal pattern (Fig. 11). The choice of actuator locations shown in Fig. 12 came as a result of some preliminary numerical experimentation based on placing each of the actuators at a controllability peak. For that choice, sequential synthesis invariably produced very high damping ratios in mode 1 and very low damping in mode 5, which has a nodal line (zero controllability) passing through the actuator located at CP4. On the basis of these numerical observations, the actuators at CP2 and CP5 were relocated on each side of CP5, as shown in Fig. 12. With this arrangement, actuators No. 1, 2, and 3 control the double-root mode 4-5, with actuator No. 2 also controlling mode 2 in a slightly suboptimal fashion.

4) The sequential synthesis process shown in Table 6 reveals that mode 5 is still the most difficult to control. At iteration step No. 9, 10 percent damping (at least) is achieved in all five modes. The next three iterations serve only to distribute the damping more equally between these modes, and in particular to reduce the

42.4 percent damping in mode 1. At this point, lack of a more specific control objective begins to matter because the synthesis could proceed in any of several ways. LAC systems are not particularly appropriate for specific (relatively high) modal damping requirements in selected modes, and other techniques (high-authority control, HAC) ought to be used. It is precisely in the context of such other controllers that LAC systems are useful, i.e., they provide broadband damping (in many modes) to absorb the destabilizing spillover of the other mode-specific controllers.

5) The sequential choices for the modal weights W_n and desired dampings ζ_n at each iteration step in Table 6 reveal a process which is characteristic of all optimal control synthesis processes, i.e., the heuristic adjustment of weights (occurring in the cost function) vis-a-vis the control gains obtained. (For LACSYS, the desired dampings, in a sense, also play the role of weights.)

PROOF-MASS ACTUATORS

Proof-Mass Actuator Concept

The application of forces to a structure in space can be achieved by three principal means:

1) Intrastructural actuators, pushing one element of the structure against another (e.g., member dampers)
2) Inertial reaction actuators, which create a force on the structure by reaction against a separate mass element which may either be discarded, as in the case of jets, or kept connected to the structure, as in the so-called "proof-mass" actuators
3) Environmental actuators (e.g., magnetic, solar, etc.) obtained by interaction of the actuator with the environment

Although any of these methods could theoretically be used for the control of structures, practical considerations will help suggest the most likely candidate for each application. Type 3 may be discarded first because the force levels involved would usually be too low. Type 1 is very straightforward and is useful in many cases. However, it has two important drawbacks: first, because of its intrastructural nature, it tends to push energy around in the structure, and second, in the case of large structures, "member dampers" for instance will have to be of such size that their own flexible characteristics will come into play and add to the complexity of the problem. As for type 2, the jet solution may not be acceptable for various reasons: excitation of higher modes, difficulty of implementation, contamination of sensitive surfaces, fuel storage, etc.

Thus, the best actuator is a momentum exchange device. In a previous study Ref. [1], the use of control-moment gyros (CMGs) was discussed and analyzed. These devices are capable of imparting very large torques to a structure and thereby absorbing significant amounts of vibrational energy. Although there does not

exist an (exact) linear momentum counterpart of the angular momentum storage devices, the "proof-mass" actuator comes closest to the linear analog of a gyro.

The important characteristic to be remembered is that the force f applied to the structure is the opposite of the force acting on the mass m of the actuator, and thus this mass will accelerate with the acceleration - f/m. Therefore, unless the force is reversed, the mass will continue to travel. This seems an obvious point, but it is an important distinction from the CMG case, where the gimbal angle stays constant when no torque is generated. This means that proof-mass actuators cannot be used for rigid-body control; their main purpose is to control vibrations, since in this case they will produce a force with no DC content. In fact, in practical implementations, these actuators will always be AC coupled to remove any possible bias, and also the mass will have to be physically restrained by a weak spring so it would not drift.

This being established, proof-mass actuators can apply a very significant amount of vibrational forces to a structure, and conversely, absorb significant amounts of vibrational energy with the proper feedback loops. They have the great advantage of easy implementation, since they are self-contained and can be attached almost anywhere to a structure. Their only drawback is that they are not currently available in space technology.

Active Versus Passive Damping

The distinction between active and passive damping may seem very academic at first. Indeed, let y be the displacement of a point in the structure, then local damping may be introduced by applying a force

$$f = - D\dot{y}$$

Now, whether D is due to the viscosity of a dashpot liquid, eddy currents, or an actuator-electronic compensator combination, makes no difference to the result. For space applications, however, it is easier to use electromechanical actuators

than hydraulic or friction systems which are not very reliable. Also, values of D can be adjusted very easily in the electronics so that values may be achieved that are not obtainable with mechanical systems. Thus, except for these few points just mentioned, there does not seem to be a real issue. However, the situation becomes quite different when one considers how the force f is generated, and for proof-mass actuators it makes a difference.

Consider the simple case depicted in Fig. 13. The actuator produces a force f on the structure and a reaction force -f on the mass m. The displacement of the structure at the actuator location is y, and the relative displacement of the proof-mass with respect to the structure is x. The dynamic equation of the proof-mass is then

$$m(\ddot{x} + \ddot{y}) = -f . \tag{71}$$

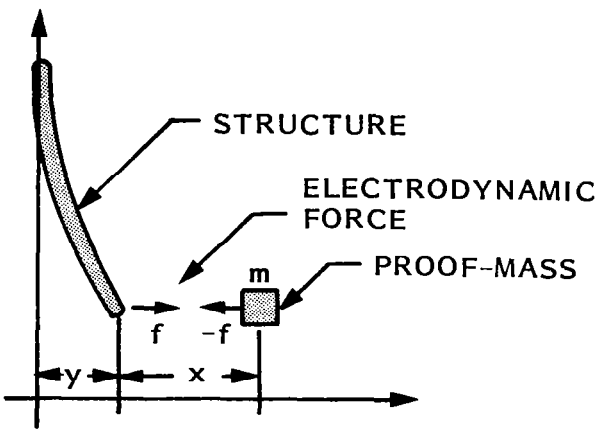

Fig. 13 Proof-Mass Actuator Acting on Portion of Structure

We will consider two cases:

1) Passive Damping

The force f is generated by viscosity, eddy currents, or other passive means, and may be written as

$$f = D\dot{x} \tag{72}$$

Using Eqs. (71) and (72), the transfer function may be obtained

$$f/y = \frac{-mDs^2}{ms + D} \tag{73}$$

Equation (73) does not exactly represent a pure rate feedback; only when $s >> D/m$ is it approximately one

$$f/y \cong -Ds$$

Now assume that damping needs to be introduced at some frequency $\omega/2\pi$. Letting $s = i\omega$ in Eq. (72) leads to

$$f/y = \frac{mD\omega^2}{D + im\omega}$$

Thus, the imaginary part (i.e., the one which will actually contribute to damping) is

$$(f/y)_{damping} = -\left[\frac{m^2 D\omega^2}{D^2 + m^2\omega^2}\right] i\omega \equiv -D'(D)\, i\omega \tag{74}$$

The next question is: how much damping is achievable? Equation (74) shows that the function $D'(D)$ vanishes both at 0 and infinity, and has a local maximum at $D = m\omega$, where the equivalent damping gain is $D'_{max} = 1/2\, m\omega$. Since the equivalent feedback law around the frequency ω has the form

$$f = -D'\dot{y} \tag{75}$$

the damping introduced by the passive device is limited.

2) Active Damping

Can this limitation be removed by active damping? If active damping meant merely to replace the mechanical gain D in Eq. (72) by an electronic one, the answer would obviously be no. However, active damping means also that sensing may be done differently. In this case, it is possible to sense y directly, rather than the natural "sensing" of x occurring in a dashpot.

Thus, the control law, Eq. (72), can be replaced by

$$f = -D\dot{y} \qquad (76)$$

and in this case, there is, at least theoretically, no limit on what D could be, in opposition to the passive case in Eq. (75).

Linear Proof-Mass Actuators

A first attempt to build a proof-mass actuator was made using a linear electromagnetic actuator (the Ling shaker model 102) which normally is used to shake structures from a ground base (see Table 7 for specs).

Table 7. LING 102 CHARACTERISTICS

Weight:	1.1 kg
Max. Force Output:	7 N
Max. Travel:	$\pm$ 3 mm

This actuator consists mainly of a powerful, heavy, permanent magnet and a cylindrical coil free to move in the magnet gap and attached to an output rod, as shown in Fig. 14. A bellows-type suspension system maintains the coil centered, while allowing for small axial motions. Because the magnet and its casing are heavy, this assembly is used as the proof-mass, while the output rod is attached to the structure being controlled.

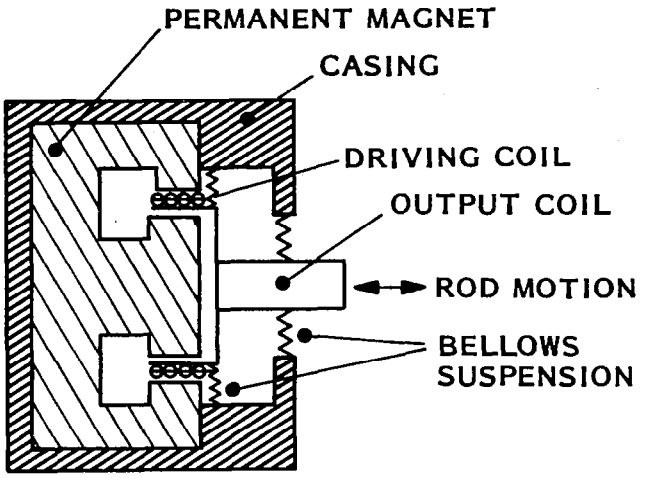

Fig. 14 Simplified Cross Section of Ling Shaker Model 102

There are two problems to solve before actually using this type of actuator:

1) The bellows suspension is quite stiff and tends to stick at low force levels, so that the (force output)/(current input) transfer function is nonlinear, both in frequency and amplitude
2) Despite this stiffness, it is yet incapable of holding the weight of the magnet in the gravity field, and is especially weak in off-axis directions

In order to solve the second problem, a cradle had to be built to hold the output rod in a quasi-rectilinear path (Fig. 15). This is not really good mechanically because the coil does not exactly translate and thus may come into contact with the magnet for large motions. As for the suspension stiffness and stiction, which is aggravated by the cradle system because of misalignments and approximate linear motions, nothing much could be done mechanically, short of redesigning the whole actuator and centering system.

However, one interesting solution was to wash out the actuator pathologies by introducing a feedback loop around the actuator. Ideally, the force output f should be a linear function of the input current. One possibility is then to measure this force (say by load cells) and feed it back to the actuator after comparison with the

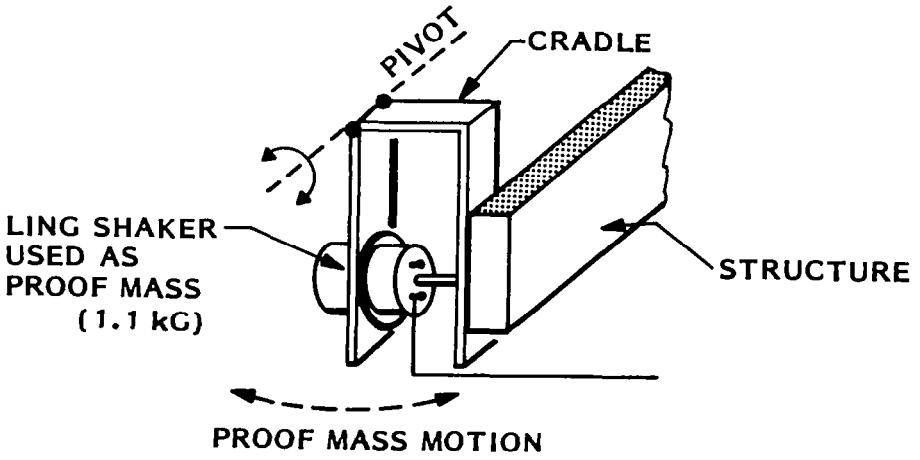

Fig. 15 Pivoted Cradle Suspension for Ling Shaker

input command. It turns out, however, that this method is not easy to implement practically. Another solution was thus developed which consists in controlling not the force, but the velocity of the output.

Velocity-Controlled Actuators

In order to eliminate undesirable dynamic characteristics of the actuator, the velocity of the output rod of the actuator is controlled by the feedback loop shown in Fig. 16.

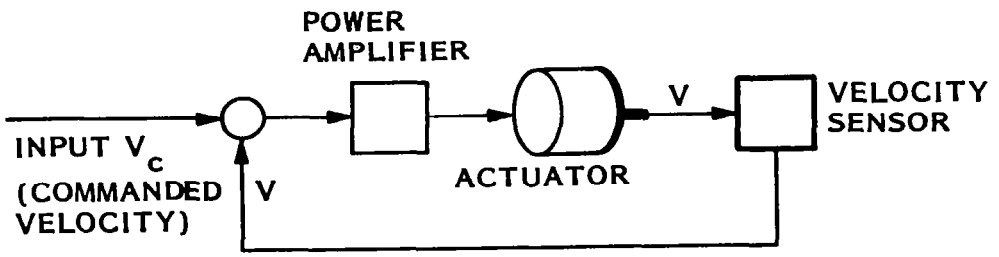

Fig. 16 Actuator Feedback Loop

Let m be the mass of the proof mass, k the stiffness of the suspension system, and x the relative displacement of the output rod. The rod is attached to some structure where displacement is denoted by y. Thus, the equations of the system, in the s-plane are

$$\left.\begin{aligned} ms^2 (x + y) + kx &= - f + G (v_c - v) \\ v &= sx \\ y &= z(s)f \end{aligned}\right\} \tag{77}$$

where z(s) is a transfer function characteristic of the structure. If the structure is very rigid, z(s) is very small in the frequency range of interest (e.g., the actuator mounted on a test bench). Solving Eq. (77) for v gives the transfer function

$$v/v_c = \left[1 + \frac{k + ms^2}{Gs\ (1 + ms^2\ z(s))}\right]^{-1} \tag{78}$$

Thus, for G large enough, the influence of m, k, and z are washed out and v basically follows the commanded velocity v_c. The bandwidth of such systems is basically given by

$$\omega_o \sim G/m \tag{79}$$

and the minimum achievable velocity is given by

$$v_o = f_o/G \tag{80}$$

where f_o is the friction force in the actuator system. Thus linearity in both frequency response and amplitude is greatly improved by the velocity feedback. (Typical examples will be seen subsequently in Fig. 20.)

In the case of the Ling shaker, it is possible to sense the velocity by measuring directly the back emf of the driving coil with an impedance bridge, as shown in Fig. 17. The advantage of this method is that it does not require additional hardware. However, the adjustment of the bridge may be difficult to achieve because of temperature drifts, especially when the power dissipation is large over a period of time.

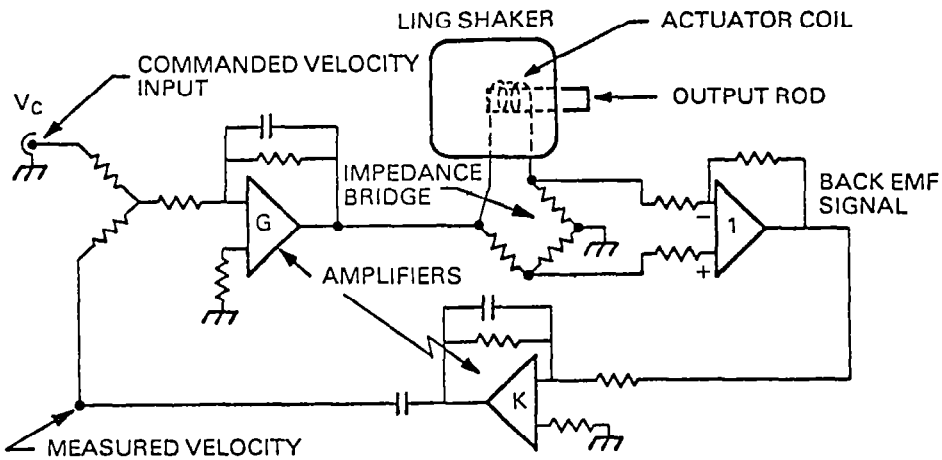

Fig. 17 Velocity-Controlled (VC) Actuator Electronics for Ling Shaker Model 102

Velocity-controlled (VC) actuators are quite different from force actuators and thus must be used differently. For LAC implementation, the usual control law in its simplest form is

$$f = -D\dot{y} \tag{81}$$

If the structural displacement y is relatively small compared to the displacement of the proof-mass*, then

*This is normally the case because the structure's generalized mass is usually larger than the mass of the proof-mass.

$$f \cong -m\ddot{x} \qquad (82)$$

and thus Eq. (81) may also be written as

$$\ddot{x} \cong \frac{D}{m}\dot{y} \qquad (83)$$

and integrating once leads to

$$v \cong \frac{D}{m}y + \text{constant} \qquad (84)$$

This shows that the velocity of the actuator must be proportional to the structural displacement. Therefore, when using a VC actuator, one should feedback position and not rate as was the case for force actuators. This is an unusual, but very important point to be noted. Another way to look at it is to consider the electronic compensator shown in Fig. 18.

The commanded force f_c goes through a gain $-1/m$ and is then integrated before going to the VC actuator. The velocity of the proof-mass is then $v = -f_c/ms$ and the force output is $f = -msv = f_c$. Thus the integrating circuit has transformed the VC actuator into a force actuator. In practical applications, however, it is important to remember that proof-mass actuators must be ac coupled, and thus the integration in Fig. 18 must be replaced by a compensation of the type $s/(s + a)(s + b)$, where a and b are small compared to the frequency of the lowest mode to be controlled.

Pivoted Proof-Mass (PPM) Actuators

Linear actuators are plagued by three main disadvantages: considerable weight, stiff guiding/suspension systems with inherent friction, and weakness of that system in transverse loadings. K. Silveira developed a new actuator concept at Lockheed in 1975 for fast mirror actuation to eliminate these pathologies.

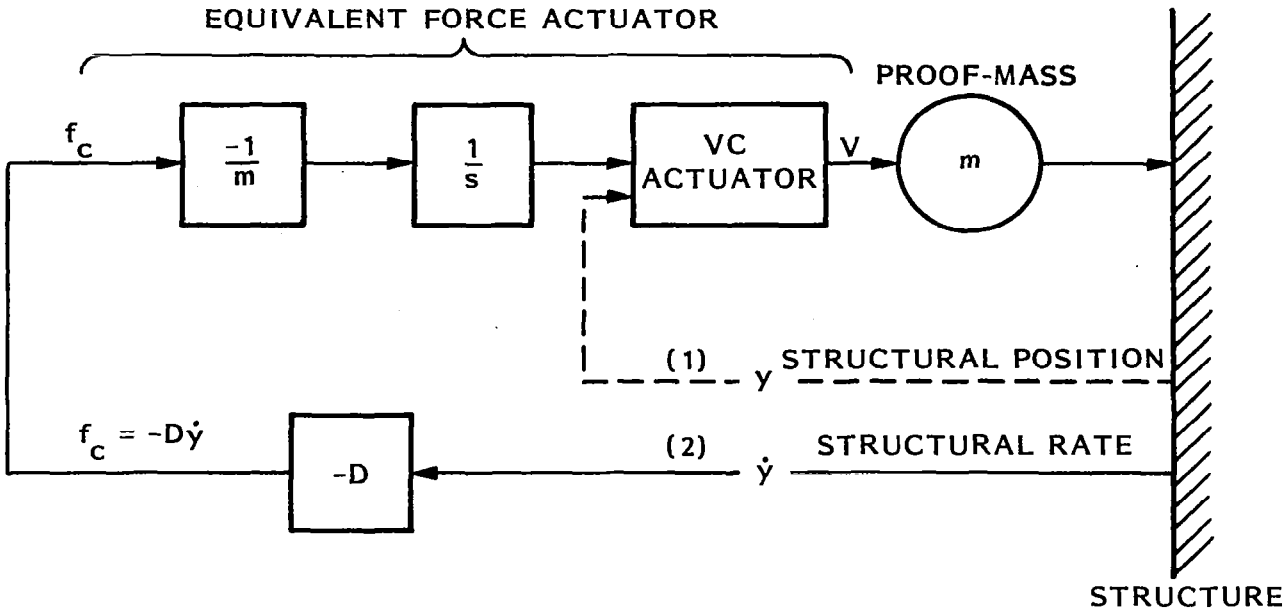

(1) DIRECT USE OF VC ACTUATOR

(2) USE OF VC ACTUATOR AS A FORCE ACTUATOR

Fig. 18 Electronic Compensation for Velocity-Controlled (VC) Actuators

This concept was modified and adapted by J. Aubrun to the present pivoted proof-mass (PPM) actuator. In this actuator the linear motion of the proof-mass is approximated by a small circle of arc about a pivot point realized by a flexure. This type of flex-pivot has three advantages: 1) it is very strong in transverse loadings, 2) it has no stiction, and 3) it is mechanically extremely accurate. The actuation is obtained by a light electrodynamic motor. Figure 19a shows a picture of an actual PPM prototype and Fig. 19b a schematic of the device. Velocity feedback is used also with this type of actuator. Figure 20 shows the open- and closed-loop transfer functions of the actuator.

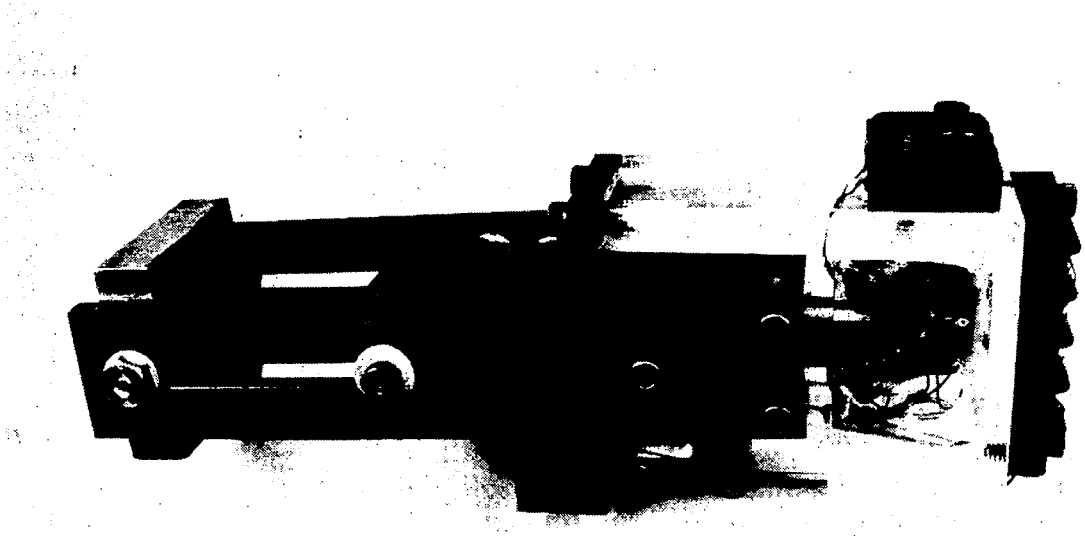

a. Prototype of PPM Actuator

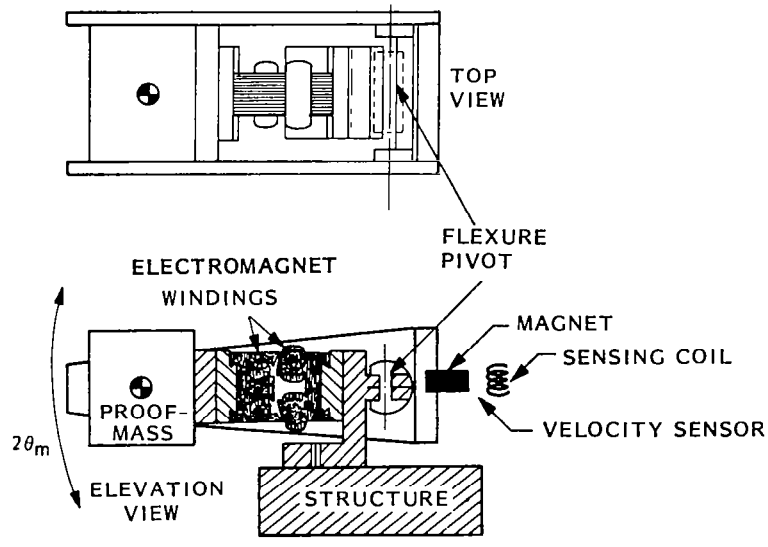

b. PPM Actuator Schematic

Fig. 19 Pivoted Proof-Mass (PPM) Actuator

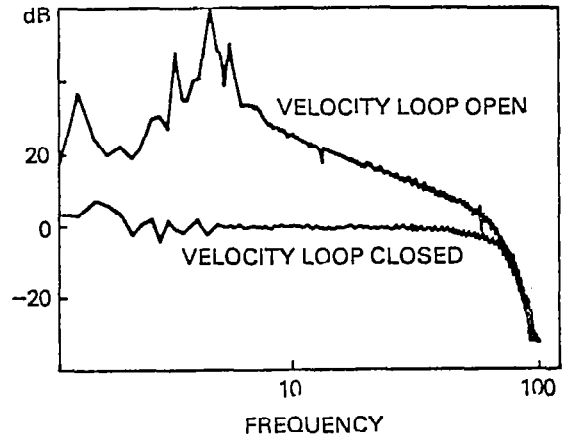

Fig. 20 Open- and Closed-Loop Transfer Functions of a Velocity-Controlled PPM Actuator (Output Velocity Versus Commanded Velocity)

The dynamics of the PPM actuator are not as straightforward as for the linear type. A dynamic model of the actuator is shown in Fig. 21.

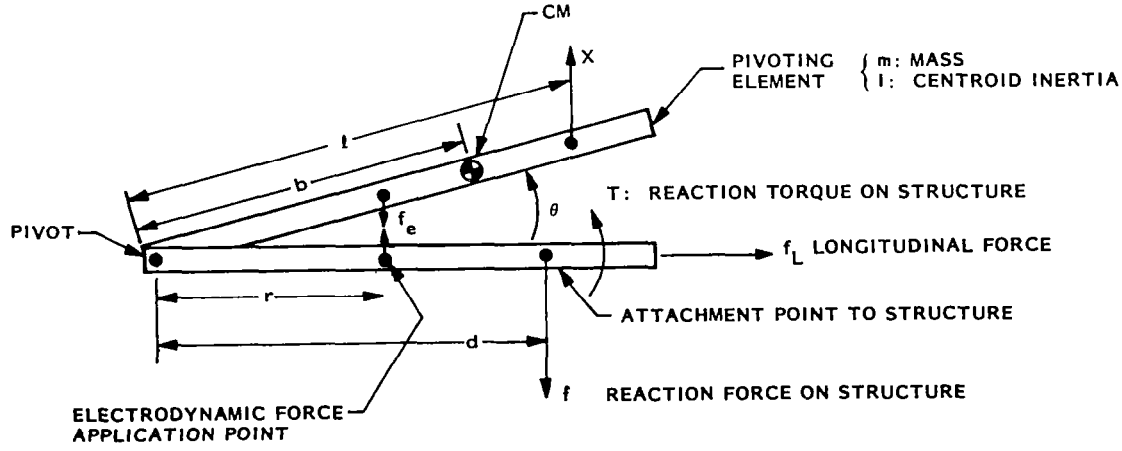

Fig. 21 PPM Actuator Dynamics Model

Because of the pivoting, both reaction force and torque are produced on the structure. Application of D'Alembert's principle shows that

$$\left.\begin{aligned} f_L &= -\,mb\,(\dot{\theta}^2 \cos\theta + \ddot{\theta}\sin\theta) \\ f &= mb\,(\ddot{\theta}\cos\theta - \dot{\theta}^2 \sin\theta) \\ T &= (I + mb^2)\,\ddot{\theta} - mbd\,(\ddot{\theta}\cos\theta - \dot{\theta}^2 \sin\theta) \end{aligned}\right\} \qquad (85)$$

Since the angular displacement θ is usually limited to a few degrees, the above equations may be conveniently linearized. The longitudinal force f_L may be ignored so that the force and torque applied to the structure by the actuator are given by

$$\left\{\begin{aligned} f &\cong mb\,\ddot{\theta} && (86) \\ T &\cong (I + mb^2 - mbd)\,\ddot{\theta} && (87) \end{aligned}\right.$$

where (see Fig. 21):

$$\ddot{\theta} = \frac{rf_e}{I + mb^2} \qquad (88)$$

Equation (87) shows that it is possible to have no torque transmitted to the structure by choosing the attachment point at the distance

$$d_o = (I + mb^2)/mb \qquad (89)$$

Varying d above or below this value will change the sign of the output torque as well as its magnitude. The mass of the PPM actuator and its CM may be adjusted by changing the position and mass of a lead piece situated at the distance ℓ from the pivot point.

Let b_o, m_o, and I_o be, respectively, the position of the CM, the mass, and the inertia with aspect to the pivot of the "unloaded" actuator, and m_1 the mass of the lead piece with which it is loaded. Then

$$\left.\begin{aligned} m &= m_o + m_1 \\ b &= \frac{m_o b_o + m_1 \ell}{m} \\ I + mb^2 &= I_o + m_1 \ell^2 \end{aligned}\right\} \tag{90}$$

and using Eqs. (86) and (88) shows that

$$f/f_e = \left(\frac{1 + m_o b_o / m_1 \ell}{1 + I_o / m_1 \ell^2} \right) \frac{r}{\ell} \tag{91}$$

PPM Scaling Laws

We must consider two important parameters in the design and use of PPM actuators besides the mass/inertia properties mentioned previously:

(1) f_{em} = maximum electrodynamic force
(2) θ_m = maximum angular displacement

Since the angular displacement θ depends upon the frequency, optimal choices for the design parameters will depend upon the frequency range of application. From the two conditions

$$|f_e| \leq f_{em} \tag{92}$$

$$|\theta| \leq \theta_m \tag{93}$$

and Eqs. (86), (90) and (91), two new conditions are found:

$$|f| \leq \left(\frac{1 + m_o b_o / m_1 \ell}{1 + I_o / m_1 \ell^2} \right) \frac{r}{\ell} f_{em} \tag{94}$$

$$|f| \leq (1 + m_o b_o / m_1 \ell)\, m_1 \ell\, \omega^2\, \theta_m \tag{95}$$

when $\omega/2\pi$ is the frequency of the output force.

Design regions may be derived from these conditions. The quantities ℓ/r and ω may be chosen as main parameters and regions of possible values of f plotted as functions of them. Typical plots were obtained for a prototype PPM actuator whose characteristic parameters are shown in Table 8.

Table 8. CHARACTERISTIC PARAMETERS OF PROTOTYPE PPM ACTUATOR*

Mass	Geometry	Electrodynamic
$I_o = 1.5\ 10^{-5}$ kgm^2	$b_o = 0.016$ m	
$m_o = 0.088$ kg	$r = 0.021$ m	$f_{em} = 1$ N
	$\theta_m = 0.067$ rad	

Two cases were studied, for two different design values of the proof-mass m_1: 0.08 and 0.16 kg, respectively. Results for design #1 are shown in Figs. 22 and 24, and for design #2, in Figs. 23 and 25. Figures 22 and 23 show the output force f as a function of ℓ/r. Depending on the lever arm, more or less force can be obtained. The zero point (obtained for a negative value of ℓ) corresponds to the composite center of mass being at the pivot point.

*Prototype actuator (design #1) delivered to Dr. G. C. Horner, Langley Research Center.

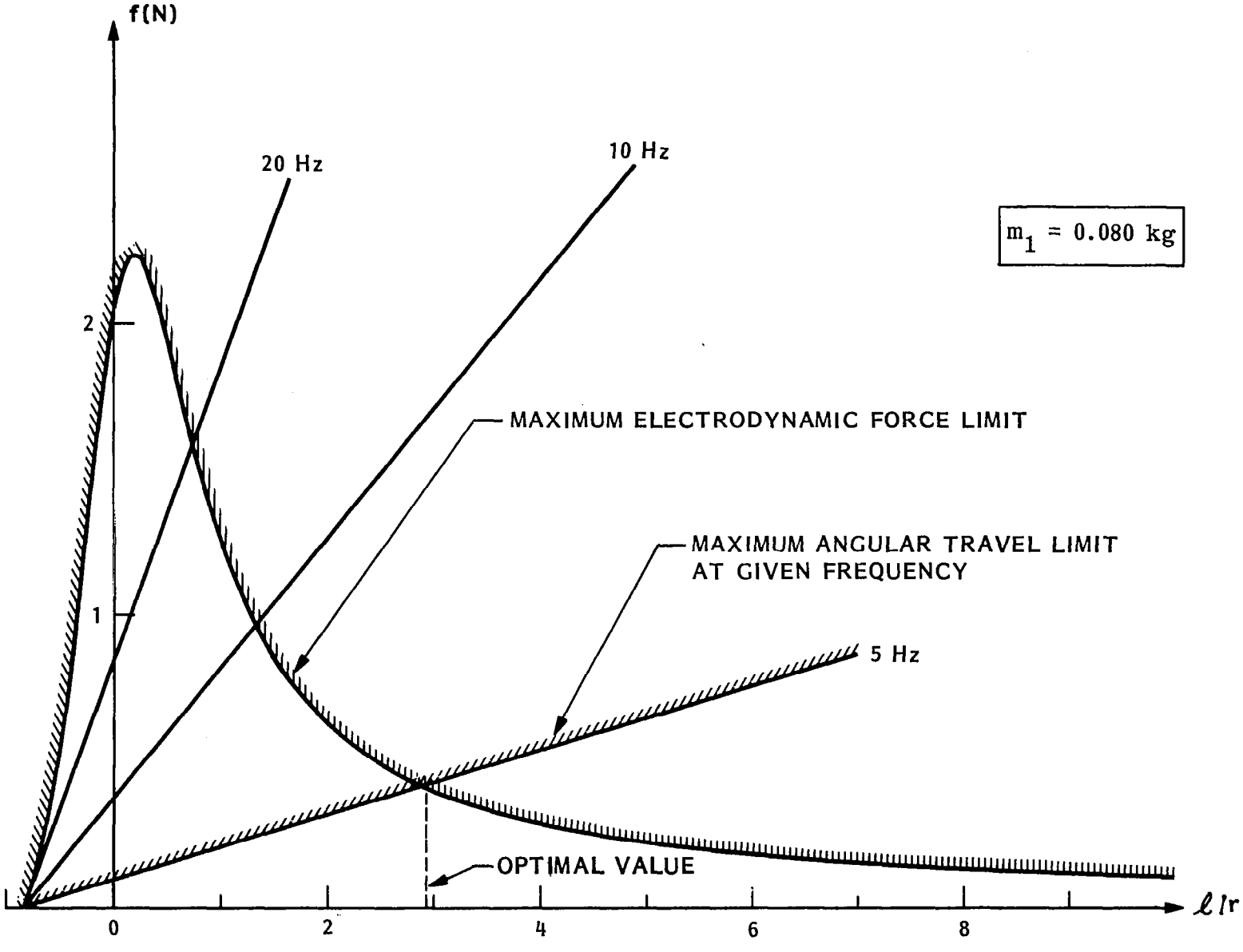

Fig. 22 PPM Actuator Design #1 – Performance Region (f, ℓ)

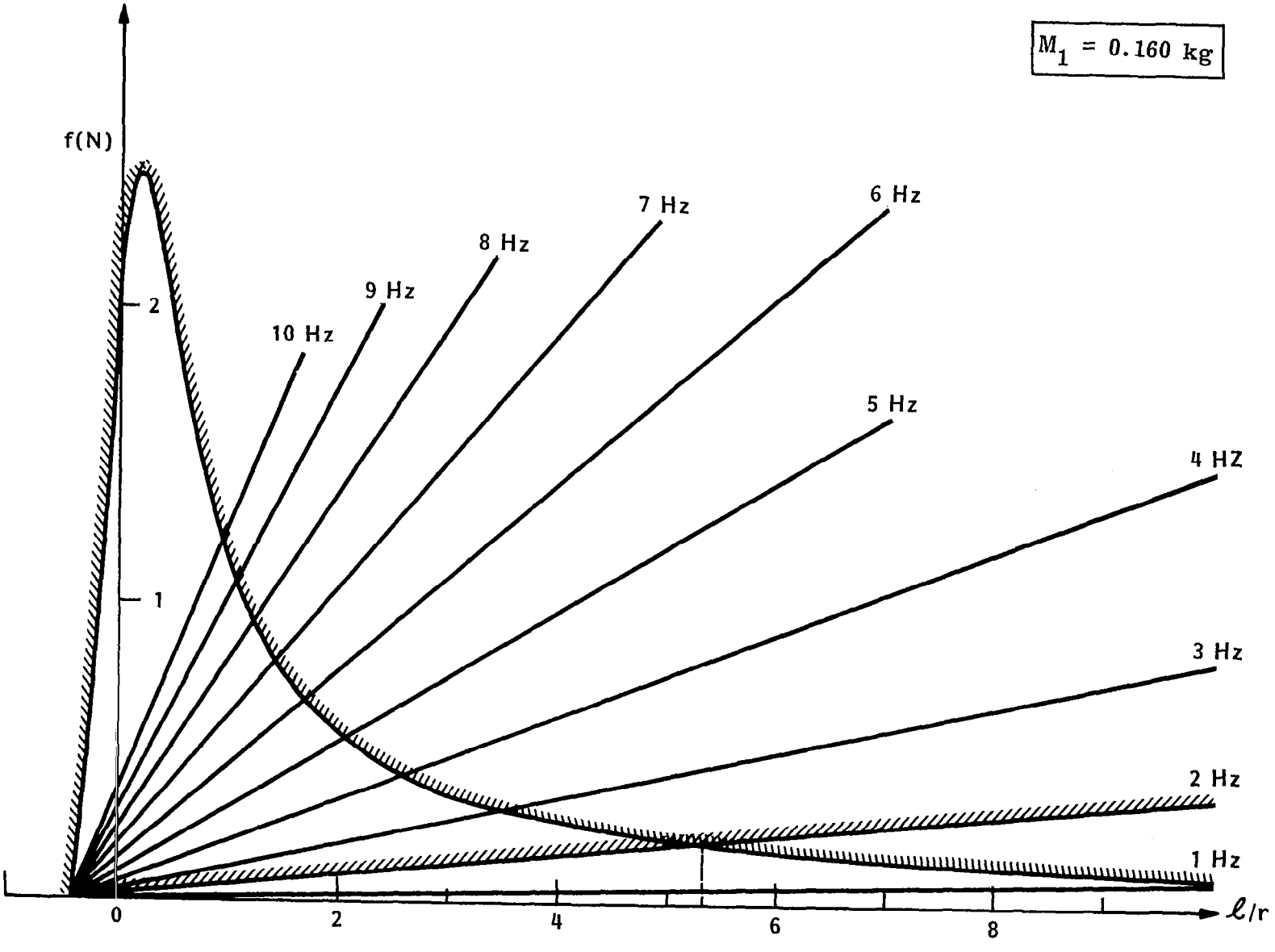

Fig. 23 PPM Actuator Design #2 – Performance Region (f, ℓ)

The fact that the curves in Figs. 22 and 23 do not go to infinity for $\ell/r = 0$ but have a maximum is due to the inertia of the unloaded actuator which absorbs part of the energy going to the proof-mass m_1. The straight lines represent the limits, at various frequencies, due to the angular travel limitation. It is thus seen that at a given frequency, there is an optimum value for ℓ/r, corresponding to the intersection of the curve and the straight line. If this value of ℓ/r is chosen for a given frequency, then the actuator will perform properly at all higher frequencies. For instance, if actuator (design) #1 has to control vibrations at or above 5 Hz, a value close to 3 is optimal for ℓ/r. In this case, design #1 will lead to the values:

$$\left.\begin{aligned} \ell &= 0.062 \text{ m} \\ b &= 0.038 \text{ m} \\ m &= 0.168 \text{ kg} \\ I &= 8.2 \times 10^{-5} \text{ kg m}^2 \end{aligned}\right\} \text{ optimal for 5 Hz} \qquad (96)$$

The effect of increasing the mass m_1 is to push up the angular travel limit, as can be seen by comparing Figs. 22 and 23, thus allowing the actuator to work at lower frequencies with basically the same force output. Obviously the increase in mass can be traded off against an increase of ℓ/r, but at the expense of the force level. For instance, to work efficiently at 2 Hz and above, actuator (design) #2 should have a value of ℓ/r of about 5.3.

Another set of curves is shown in Figs. 24 and 25 where f is plotted against the parameter $m_1 \theta_m (\omega/2\pi)^2$. Again the two limits (maximum electrodynamic force, maximum angular travel) define a usable region which is, this time, a function of ℓ/r. The frequency scale is also shown on the top of the plot. These plots show that above a certain frequency, the maximum force output becomes constant. The intersection of the two limits corresponds to the optimal frequency, for a given value of ℓ/r.

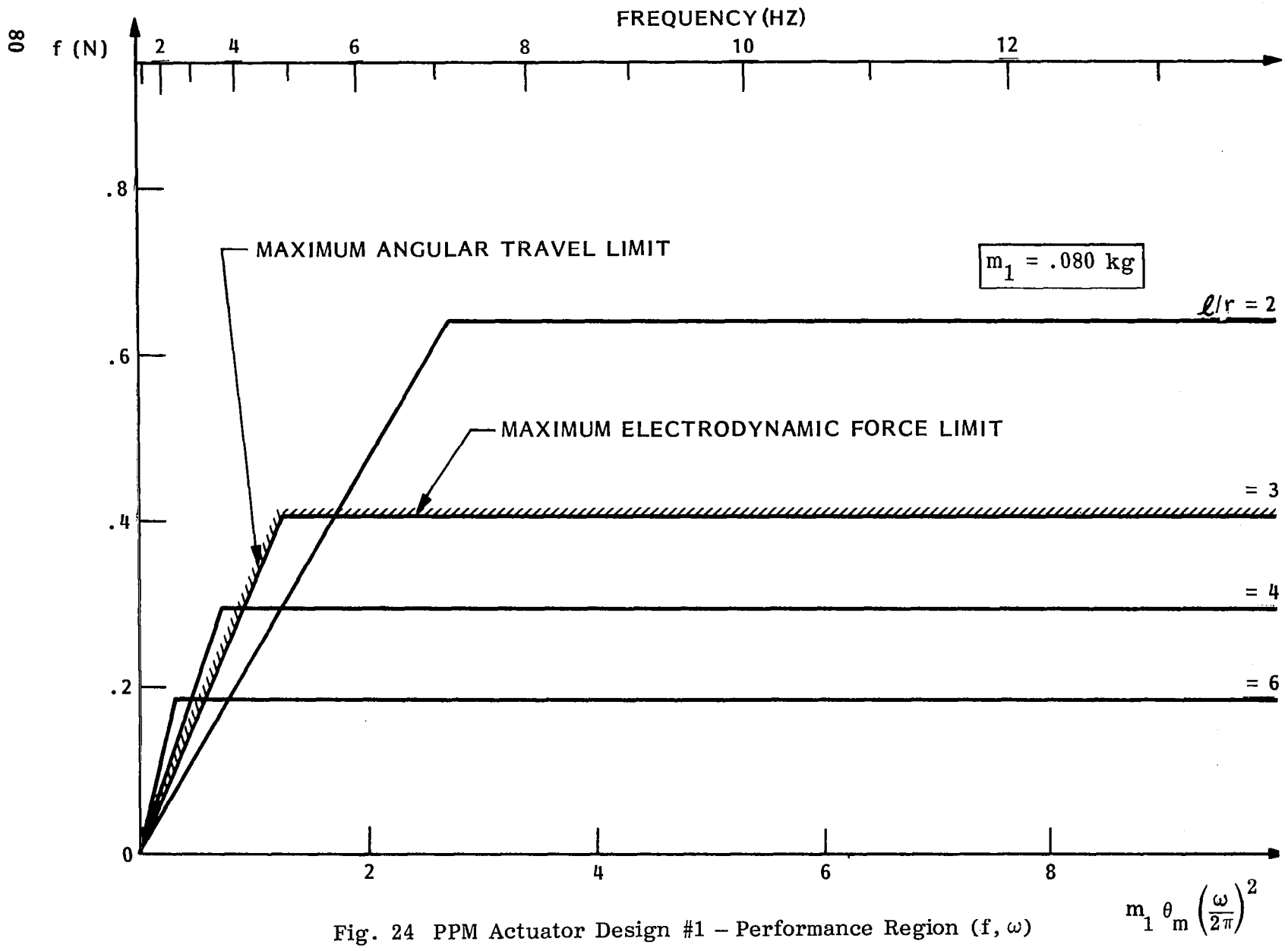

Fig. 24 PPM Actuator Design #1 – Performance Region (f, ω)

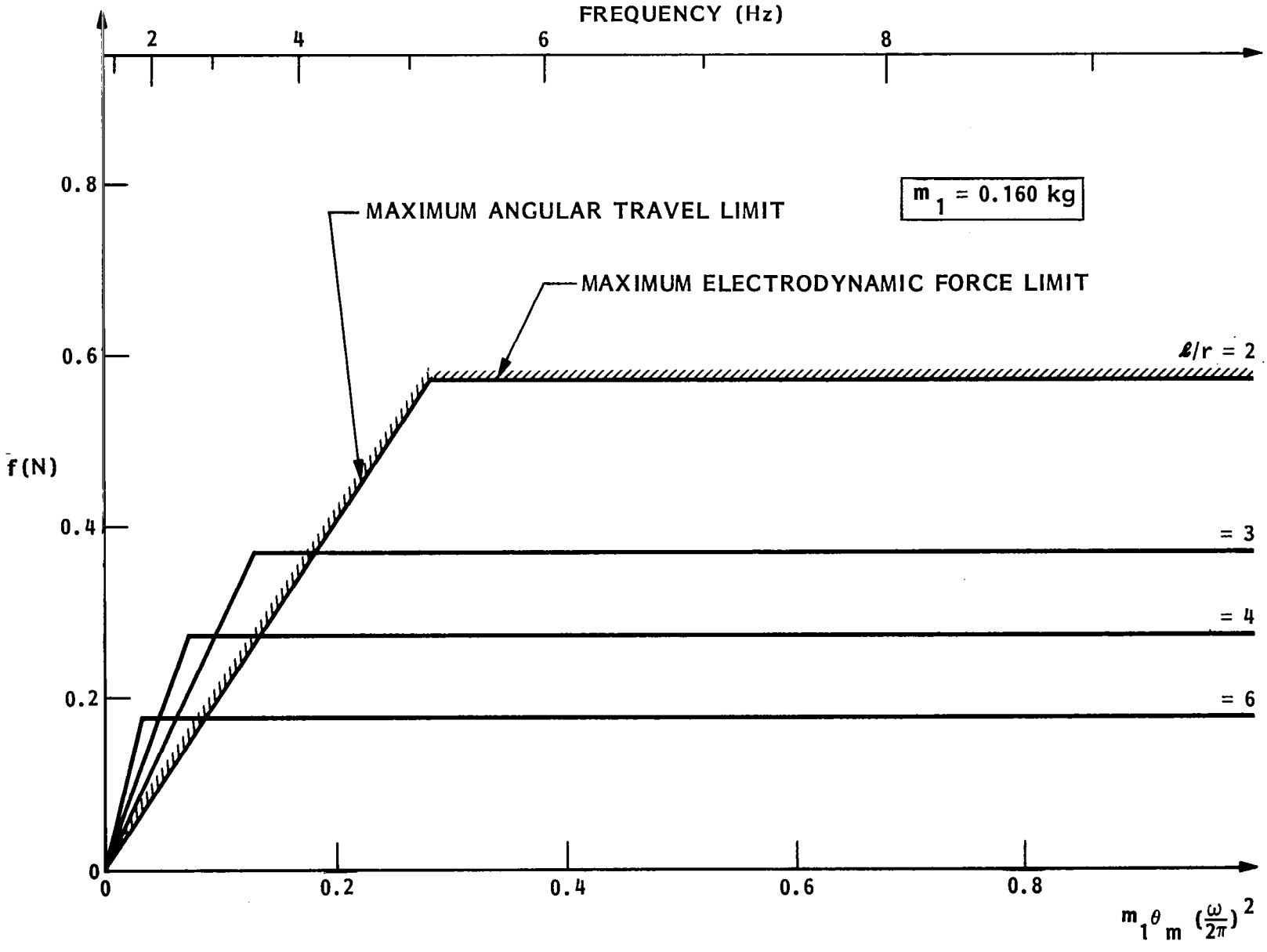

Fig. 25 PPM Actuator Design #2 – Performance Region (f, ω)

The optimal lever arm (ℓ/r) can be obtained from Eqs. (94) and (95), i.e.,

$$(\ell/r)_{opt} = \left(\frac{f_{em}}{m_1 r \theta_m \omega^2} - \frac{I_o}{m_1 r^2} \right)^{1/2} \tag{97}$$

This expression, which defines the abscissa of the intersection of the curve defined by Eq. (94) and the straight line defined by Eq. (95), is only valid if this intersection is on the right of the peak of the curve. Otherwise, the peak itself is the maximum value for f, in which case ℓ/r is given by

$$(\ell/r)_m = \frac{m_o b_o}{m_1 r} \left[\left(1 + \frac{m_1 I_o}{m_o^2 b_o^2} \right)^{1/2} - 1 \right] \tag{98}$$

Corresponding to Eqs. (97) and (98), the values of f are, respectively, given by

$$f_{opt} = \left[m_o b_o + r m_1 (\ell/r)_{opt} \right] \omega^2 \theta_m \tag{99}$$

$$f_m = \frac{1}{2} \frac{1}{(\ell/r)_m} f_{em} \tag{100}$$

As was done in a previous study (Ref. [1]) for gyrodampers, scaling laws may be derived by considering geometric scaling. That is, calling L a characteristic length* of the system, the following scalings are assumed:

*The parameter L is assumed to be dimensionless by letting $L = 1$ correspond to the prototype actuator (design #1) described in Table 8, p. 76.

$$\left.\begin{aligned} m_o &= K_m L^3 \\ I_o &= K_I L^5 \\ r &= K_r L \\ b_o &= K_b L \\ f_{em} &= K_f L^2 \end{aligned}\right\} \qquad (101a)$$

and let

$$\chi \equiv m_1/m_o \qquad (101b)$$

Thus Eqs. (97) and (98) become

$$(\ell/r)_{opt} = \chi^{-1/2} K_r^{-1} K_m^{-1/2} \theta_m^{-1/2} \left(K_r K_f (L\omega)^{-2} - K_I \theta_m\right)^{1/2} \qquad (102)$$

$$(\ell/r)_m = \chi^{-1} K_b \left[\left(1 + \chi \frac{K_I}{K_m K_b^2}\right)^{1/2} - 1\right] \qquad (103)$$

When $L\omega$ becomes larger and larger, $(\ell/r)_{opt}$ decreases, while $(\ell/r)_m$ is constant, and there is a critical value of $L\omega$ beyond which the optimal value for (ℓ/r) is given by Eq. (103) instead of Eq. (102). Correspondingly, the maximum force output of the actuator will be given by Eq. (100) instead of Eq. (99). These last two equations may be rewritten, in terms of the parameters defined by Eqs. (101), as

$$\omega^2 f_{opt} = \theta_m K_m K_b (L\omega)^4 + \left(\frac{K_r K_m K_f}{\theta_m} - K_m K_I (L\omega)^2 \right)^{1/2} \chi^{1/2} (L\omega)^3 \quad (104)$$

$$\omega^2 f_m = \frac{\chi K_r K_f K_b^{-1}}{2 \left(1 + \chi K_I K_m^{-1} K_b^2 \right)^{1/2} - 1} (L\omega)^2 \quad (105)$$

Equations (102) to (105) constitute the basis for PPM actuator scaling and are graphed in Fig. 26 for the values of the scaling parameters in Eq. (101a) corresponding to the prototype PPM actuator with $\chi \equiv m_1/m_o = 0.9$. These curves may be used, for design purposes, in the following way: Assuming that a value of f of the force output is required for some application at a frequency equal to $\omega/2\pi$, the value of the parameter $\omega^2 f$ is computed and plotted on the right vertical axis. Using either the f_{opt} curve (if $\omega^2 f$ is below the critical point) or the f_m curve (if $\omega^2 f$ is above it), one obtains the corresponding value of L on the horizontal axis, and hence the value of the geometric scaling parameter L. Then, for that value of L, one determines the lever arm (ℓ/r), again using either the $(\ell/r)_{opt}$ or the $(\ell/r)_m$ curve (the latter being a straight horizontal line). An example of the procedure will be given in the next section.

PPM-Damped Structure Scaling Laws

The scaling of the actuator will ultimately depend upon the structure to be controlled. Scaling laws may be derived simply from the rate feedback Eq. (76) or (81)

$$f = -D\dot{y}$$

Thus, the force amplitude at frequency ω_n is

$$f_n = D y_n \omega_n \tag{106}$$

where y_n is the vibration amplitude. According to Eq. (33), the associated damping produced by one colocated actuator/sensor pair is

$$\zeta_n = \frac{1}{2\omega_n} D \phi_n^2$$

Thus the actuator force for achieving the required damping ratio ζ_n must be

$$f_n \geq \frac{2\omega_n^2 y_n}{\phi_n^2} \zeta_n \tag{106a}$$

This relation, in conjunction with Eqs. (99), (100), (101), and (102) will allow the sizing of the required actuators. Although it is not practical or even possible to define scaling laws for a general structure/actuator system, some insight may be gained by considering a simple structure and observing the evolution of the different parameters as mass and length are changed. For that purpose, a free-free uniform beam damped about one axis by one PPM actuator is considered. The beam mode shape at the tip and its frequency are given, respectively, by

$$\left.\begin{aligned} \phi_n^2 &= 4\, M_s^{-1} \\ \omega_n &= \beta_n^2\, M_s^{-1/2}\, L_s^{-3/2}\, (EI_s)^{1/2} \end{aligned}\right\} \tag{107}$$

where L_s and M_s are, respectively, the length and mass of the structure, β_n the root of the beam equation, and EI_s the classical stiffness parameter.

Using Eq. (106) leads to a condition on the actuator force output of the form

$$f \geq \frac{1}{2} \max_n \left(\beta_n^4 \, y_n \, \zeta_n \right) (EI_s) \, L_s^{-3} \qquad (108)$$

The 100 m graphite-epoxy beam described in Ref. [1] p. 46 will be used here as an example of application of these scaling laws. Table 9 gives characteristics of this beam from which one obtains the quantities L_s, M_s, and EI_s. Table 10 gives the value of β_n. The following problem is addressed:

Assuming that 10 percent damping is desired in the first mode of the beam, and that the vibration amplitude of the tip is initially equal to 1 cm, design a PPM actuator from the results obtained with the prototype.

Table 9 GRAPHITE EPOXY BEAM PARAMETERS

Length	$L_s = 100$ m
Outside radius	$r = 10.55$ cm
Wall Thickness	$e = 2.275$ mm
Young's Modulus	$E = 3.45\ 10^{11}$ N/m^2
Density	$\rho = 1607$ kg/m^3
Mass	$M_s = 239.7$ kg
Sectional Inertia	$I_s = 8.125\ 10^{-6}$ m^4

Table 10 FREE-FREE BEAM EQUATION ROOTS

n	β_n
1	4.7124
2	7.8540
3	10.9956
4	14.1372
5	17.2788

First, by applying Eq. (108), it is found that a force $f \sim 0.7$ N is required. Since the frequency of the first mode is 0.405 Hz,

$$\omega^2 f = 4.53$$

This value is far below the critical point ($\sim 4.2 \times 10^4$), shown in Fig. 26. Thus the set of curves shown in Fig. 27 which correspond to that lower range will be used.* These curves, $(\ell/r)_{opt}$ and f_{opt}, have been parameterized with $\chi \equiv m_1/m_o$ varying from 0.125 to 4. The value of 0.9 corresponds to the prototype PPM actuator. Using this value of χ first, the value of $L\omega$ is found to be approximately 7.3, corresponding to $L \sim 2.9$. The (ℓ/r) curve shows an optimal lever ratio of 13. If instead, one chooses $\chi = 4$, , smaller values for L and ℓ/r are obtained. These two designs are compared in Table 11, obtained from the graphically determined values of L and ℓ/r and from Eqs. (101).

Table 11 PPM ACTUATOR PARAMETERS FOR 100 m Gr-Ep BEAM

Actuator Parameters	$\chi = 0.9$	$\chi = 4$
L	2.9	2.3
ℓ/r	13.0	7.5
r	0.061 m	0.048 m
ℓ	0.792 m	0.362 m
m_o	2.146 kg	1.071 kg
m_1	1.931 kg	4.283 kg
m	4.077 kg	5.354 kg
f_{em}	8.41 N	5.29 N

*Figure 27, for $\chi = 0.9$, represents the same curves $(\ell/r)_{opt}$ and f_{opt} as appear in Fig. 26, but drawn in a neighborhood of the origin for vastly reduced values of $\omega^2 f$ and $L\omega$, and correspondingly increased values of (ℓ/r). In addition, these curves in Fig. 27 are now part of one-parameter families obtained by varying the parameter χ.

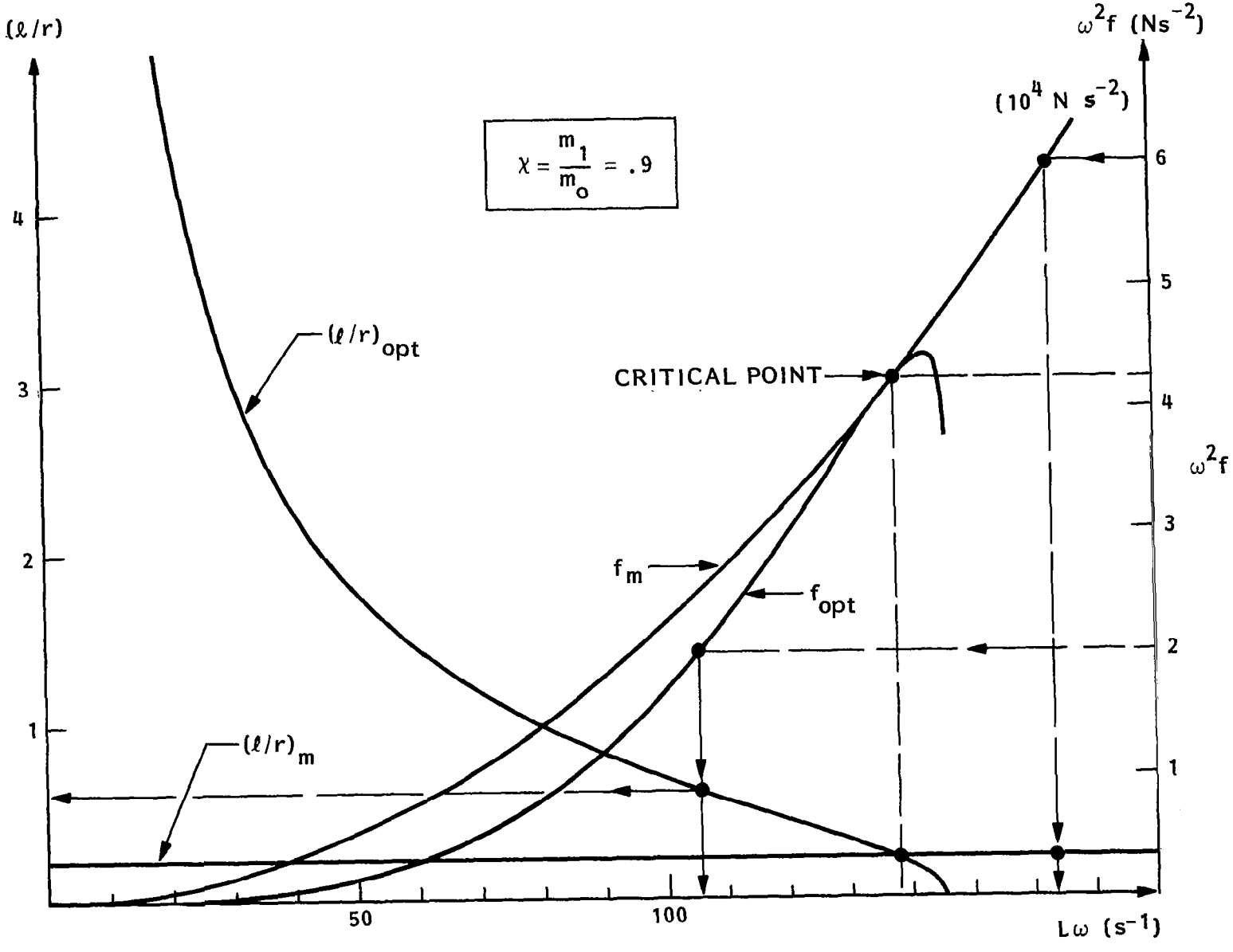

Fig. 26 PPM Actuator Design Nomograph: Force and Lever-Arm Versus Geometric Scaling Parameters

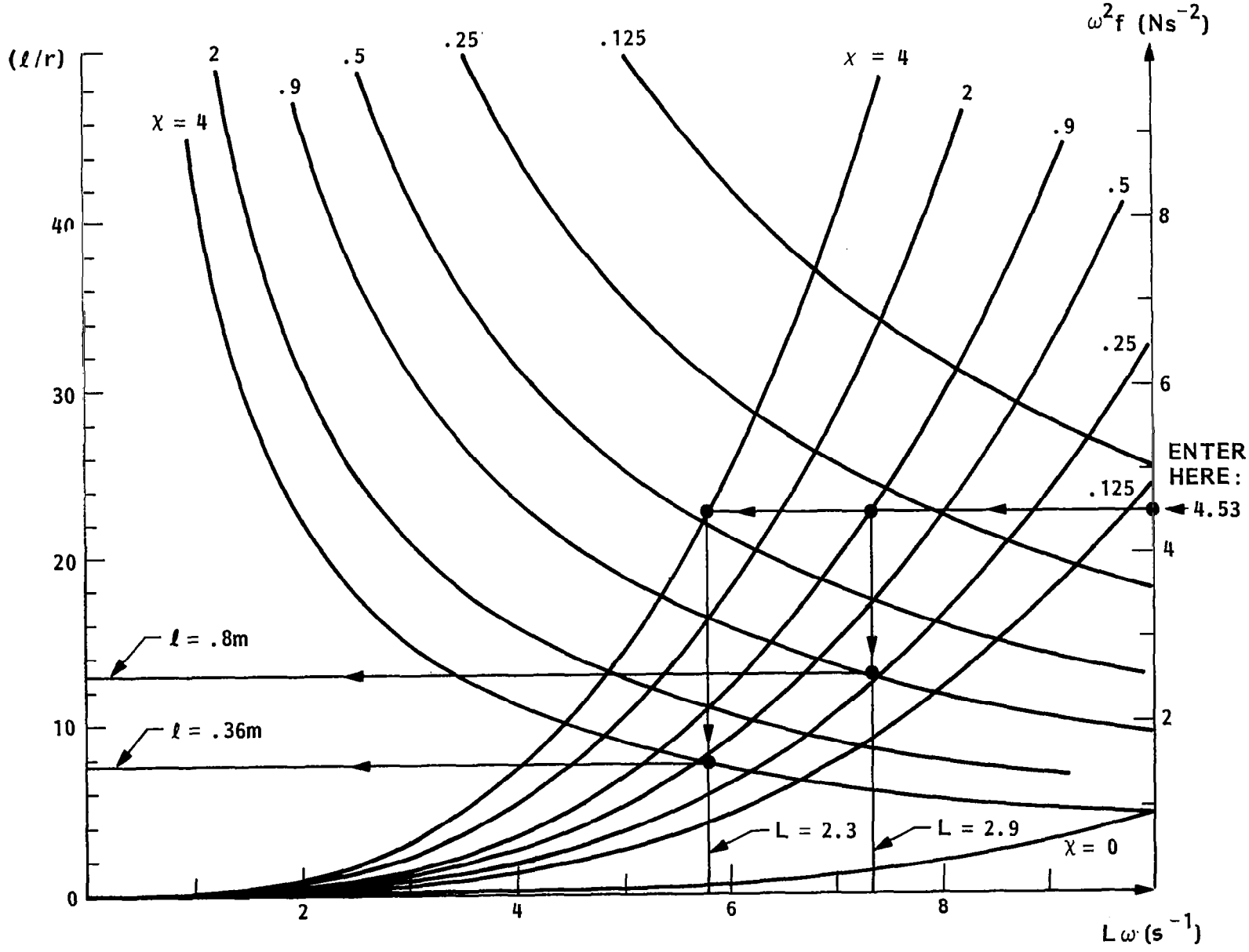

Fig. 27 PPM Actuator Design Nomograph for the 100-m Gr-Ep Beam ($\chi = m_1/m_o$ as a Parameter)

The performance of the system for higher modes can be obtained easily by Eq. (106). If it can be assumed that the modal amplitudes vary with $1/\omega_n^2$ (this corresponds to the modal content of a static deflection), then Eq. (106) shows that the maximum achievable value for ζ_n is a constant.

As can be seen, the second design, with $\chi = 4$, is a bit heavier but much smaller in size and requires a smaller electrodynamic force. It can be shown that for this particular design, and at this low end of the L_ω range, the minimum weight design is obtained for $\chi = 1/2$, in which case the total mass of the actuator is 3.977 kg. However, with $\ell \sim 2$ m, the corresponding linear dimensions become prohibitive.

CONCLUSION AND RECOMMENDATION

The analytical framework has been established for the design and gain synthesis of Low-Authority Control systems for large space structure vibration suppression and management. Design implementation of LAC systems have been illustrated for rectangular plates equipped with infinite-bandwidth sensing/actuation systems, and robustness criteria established for realistic (finite-bandwidth) actuators. A newly conceived electrodynamically driven actuator concept is given, together with an actuator control system (actuator velocity control loop) designed to minimize spurious mechanical effects which arise with any physical actuator containing some degree of structural flexibility.

The inclusion of actuator and/or sensor dynamics in these types of study can only be meaningful in the context of an experimental program in which laboratory brassboards, equipped with sensors and actuators, are used to demonstrate the mechanical implementation and performance of such LAC vibration control systems. It is recommended, therefore, that any future work in this area be strongly coupled to a laboratory experimental program in which the practical implementation issues are addressed directly. By doing so, it is hoped that a new impetus will be provided in the aerospace industry for the conception, design, and manufacture of badly needed actuator devices for large space structure vibration control.

REFERENCES

1. J. N. Aubrun and G. Margulies, Gyrodampers for Large Space Structures, NASA Contractor Report 159171, Langley Research Center, February 1979, p. 102.

2. J. N. Aubrun, "Theory of the Control of Structures by Low-Authority Controllers", J. Guid. & Control, Vol. 3, No. 5, Sep-Oct 1980, pp. 444-451.

3. J. G. Lin, "Multiple-Objective Problems: Pareto-Optimal* Solutions by Method of Proper Equality Constraints," IEEE Trans. Automatic Control, Vol. AC-21, No. 5, Oct 1976, pp. 641-650.

4. J. G. Lin, "Multiple-Objective Optimization by Multiplier Method of Proper Equality Constraints - Part I: Theory," IEEE Trans. Automatic Control, Vol. AC-24, No. 4, Aug 1979, pp. 567-573.

5. A. W. Leissa, Vibration of Plates, NASA Special Publication, NASA SP-160, 1969, VII + 353 p. (Reproduced by National Technical Information Service), publication N70-18461, U.S. Dept of Commerce, Springfield, VA 22161.

6. J. S. Przemienecky, Theory of Matrix Structural Analysis, McGraw Hill, New York, 1968, p. 316.

*Named after Vilfredo Pareto (1848-1923), an Italian sociologist and economist in Switzerland.

1. Report No.	2. Government Accession No.	3. Recipient's Catalog No.
NASA CR- 3495		

4. Title and Subtitle	5. Report Date
LOW AUTHORITY CONTROL SYNTHESIS FOR LARGE SPACE STRUCTURES	September 1982
	6. Performing Organization Code
7. Author(s)	8. Performing Organization Report No.
J. N. Aubrun and G. Margulies	
	10. Work Unit No.
9. Performing Organization Name and Address	11. Contract or Grant No.
Lockheed Missiles and Space Company, Inc. Palo Alto Research Laboratory 3251 Hanover St., Palo Alto, CA 94304	NAS1-14887-TASK 11
	13. Type of Report and Period Covered
12. Sponsoring Agency Name and Address	Contractor Report
National Aeronautics and Space Administration Washington, DC 20546	14. Sponsoring Agency Code

15. Supplementary Notes

Langley technical monitor: Garnett C. Horner
Final report

16. Abstract

This study addresses the problem of controlling the vibrations of large space structures by distributed sensors and actuators. A procedure is developed for calculating the feedback loop gains required to achieve specified amounts of damping. For moderate damping (Low Authority Control) the procedure is purely algebraic, but it can be applied iteratively when larger amounts of damping are required and has been generalized for arbitrary time-invariant systems.

17. Key Words (Suggested by Author(s))	18. Distribution Statement
Large Space Structures, vibration control, active damping, inertial actuators, control synthesis	Unclassified - Unlimited Subject Category - 39

19. Security Classif. (of this report)	20. Security Classif. (of this page)	21. No. of Pages	22. Price
Unclassified	Unclassified	98	A05

For sale by the National Technical Information Service, Springfield, Virginia 22161

NASA-Langley, 1982